Imperial College London

IMPERIAL COLLEGE LONDON

DEPARTMENT OF PHYSICS

Candidate No. 00690175

A Complexity Approach to Atrial Fibrillation

CMTH-Christensen-1

MSCI REPORT

Assessor
Dr. Tim EVANS

Supervisor
Prof. Kim CHRISTENSEN

April 25, 2015

Abstract

Atrial fibrillation (AF) is a common cardiac arrhythmia, resulting in the inefficient pumping of blood leading to other fatal conditions if left untreated[1]. The success rate of current treatment is disappointing as there is a lack of understanding of the underlying mechanism but it generally agreed that inhomogeneity in the heart is key in inducing fibrillation. Based on the existing theory that the conduction velocity (CV) of a wavefront is dependent on the connectivity of a cell[2], a hexagonal cellular automata model was devised with this feature, building upon Christensen's square model[3]. The minimum path length of a reentry circuit was found to have decreased, increasing the risk of AF. A further investigation into the effects of fibrosis (a reduction in cell connectivity)[4] was mimicked by the implementation of a patch of lower connectivity and one at a horizontally biassed percolation threshold. The patch was found to induce AF in previously zero-risk values of connectivity. Both experiments returned a higher risk of fibrillation than for previous models which lacked the extra layers of inhomogeneity.

Summary

Chapter 1 presents an introductory background into the existing research into Atrial Fibrillation (AF) and explains the motivation for the path that this report took. A brief overview of the heart's electrophysiology is presented as well as theories postulated about AF.

Chapter 2 presents the concepts of the original cellular automata model. This section also explains how fibrillation risk is measured and the reasoning behind and process of implementing a hexagonal version. Heterogeneous conduction velocity is implemented by defining a timedelay state which is directly related to a cell's connectivity. A patch was grown from the centre of the lattice and set at a lower connectivity to mimic the effects of fibrosis.

Chapter 3 presents how the model was implemented computationally addressing any boundary conditions and efficiency issues. The program was written in C++ using Visual Studio 2013. All data points were averaged over 50 simulations and run for 10^6 timesteps unless otherwise stated.

Chapter 4 presents the data obtained and the following discussion. A hexagonal lattice reduced the risk of fibrillation compared to the original square model, whilst implementing heterogeneous conduction velocity increased the risk (compared to the homogeneous hexagonal CV model). An analytical approach found that the minimum path length had decreased in a heterogeneous CV model. The patch was found to initiate fibrillation in lattices of a connectivity previously thought to be non-fibrillatory.

Chapter 5 present the conclusions and potential routes for further investigation. Given more time a continuous representation of Spector's source-sink theorem would be implemented such that the connectivity of the excited cell's next-nearest neighbours would be a factor in CV too[2]. The effects of a patch with heterogeneous CV implemented would be investigated as well. In spite of this, the overall conclusion can be drawn that heterogeneity across the heart whether it be cell connectivity or conduction velocity will increase the risk of AF. Therefore it is of importance that these effects be addressed when simulating the heart.

Declaration

The computational model was based upon ideas from an original model built by our supervisor and PhD student, K. Manani. The author and the partner gave a joint effort in building the model from scratch and in designing and implementing further features. The process of implementing new features was discussed together and then followed by individual attempts to implement and visualize it.

There was a joint effort in collecting and analyzing the data for the project up until the patch test. The author focused on running tests upon and analyzing the patch of lower ν data (section 4.3.1) whilst the partner collected and tested data for the patch at percolation threshold (section 4.3.2).

We were guided in the discussion of coming up with new features by our supervisor and PhD student, K. Manani, but the computational code was solely our work. The model was built in C++ using Visual Studio 2013, the data was compiled using Mirosoft Excel and processed using Origin Pro.

Contents

1 Introduction

Atrial fibrillation (AF) is a common form of cardiac arrhythmia and although not a fatal condition itself, it causes the inefficient pumping of blood through the body, increasing the risks of a stroke or in severe cases, heart failure[1]. Despite 800,000[1] people in the UK being affected, the underlying mechanism in AF is poorly understood and current treatment is limited in success. Research has been ongoing for the past century to ultimately reduce the risk of AF treatment as well as its recurrence rate.

1.1 Electrophysiology of the Heart

1.1.1 Heart Structure

The heart is a muscle consisting of four chambers, two lower ventricles and two upper atria. Blood enters the atria which pump it to the corresponding ventricles, where it is then pumped out to the rest of the body (figure 1).

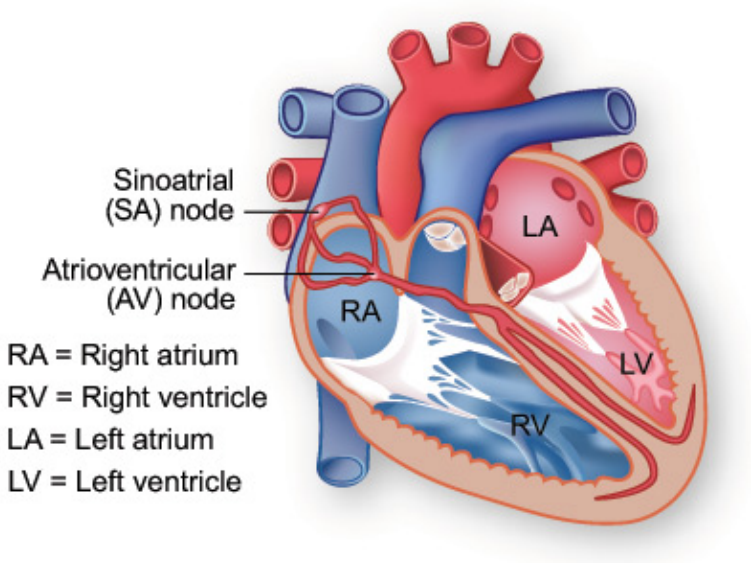

Figure 1: Diagram displaying the four chambers of the heart and the sinoatrial and atrioventricular nodes[5]. Red indicates oxygenated blood on the left side of the heart whilst blue indicates deoxygenated blood on the right.

The contraction of the atrium is normally controlled by the sinoatrial (SA) node, the heart's natural pacemaker which generates a rhythmic electrical impulse at 60 beats-per-minute (bpm), but during AF this rate increases to 400-600 bpm and the atrium undergoes rapid and chaotic contractions[6]. This impulse travels through the cardiomyocytes, an inconsistent branched network of excitable, striated muscle cells within the heart[7] causing

first, the atria to contract and then once the impulse has passed through the atrioventricular (AV) node, the ventricles too. The AV node acts as a filter only allowing a maximum of 220 impulses^{-1} [8], protecting the ventricles from high rates of atrial depolarization during AF.

1.1.2 Action Potential

The electrical impulse is the propagation of an action potential, a change in potential difference caused by the flow of Na^+, Ca^{2+}, and K^+ ions across ion-selective channels within the cardiomyocyte's membrane. The interior of an unexcited cell has an initially negative potential with respect to the exterior. It undergoes depolarization to a positive threshold potential, shortly followed by repolarization, which restores this potential to the initial resting state[8]. Together these form the action potential (figure 2) that is then propagated across neighboring cells via gap junction proteins in a ripple effect. After the initial depolarization the Na^+ channels are inactivated and the cell cannot be easily excited until full repolarization has completed, during the refractory period.

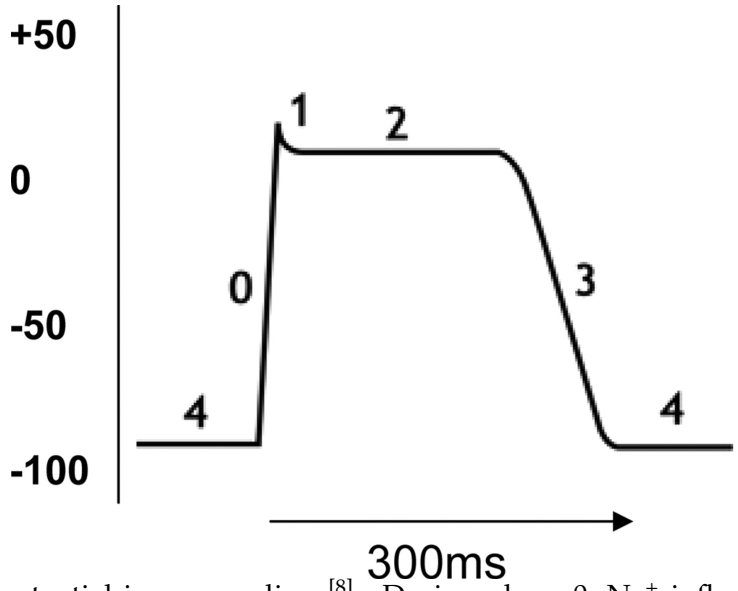

Figure 2: Action potential in myocardium[8]. During phase 0, Na^+ influx depolarizes the cell from its initial resting, unexcited potential of -90mV to +10mV. During phase 1, the membrane decreases its permeability to Na^+ and partial repolarization occurs. During phase 2, a plateau occurs as the influx of Ca^{2+} occurs, prolonging the depolarization of the cell. During phase 3, a K^+ influx repolarizes the cell whilst pumps actively restore the ion concentrations to the initial resting potential obtained in phase 4 .

1.2 Suggested Mechanisms of Atrial Fibrillation

1.2.1 Early Theories: Ectopic Foci and Circus Reentry

AF occurs when the action potentials, usually initiated by the SA node, propagate through the myocardium, the heart tissue, in an apparently random and chaotic manner. Episodes of AF can vary from short, self-terminating episodes (paroxysmal AF), which can develop into a self-sustaining condition (persistent AF) if left untreated, as the atrial tissue undergoes irreversible changes to sustain AF[6].

The first significant theory, proposed by Winterberg in 1907[9], suggested that there exist multiple ectopic foci (abnormal groups of pacemaker cells) within the heart, each generating an independent impulse and that it was the interactions of these different impulses that caused the incoordination of atrial contraction.

This was challenged by the theory of circus reentry[10][11] which proposed that within myocardium, closed circuits exist around a unidirectional anatomical block which diverts the impulse. If the pathlength (the perimeter) of such a circuit equals or exceeds the wavelength of excitation then by the time the impulse completes one circuit, the initial cells are excitable once more and the impulse continues indefinitely (figure 3b).

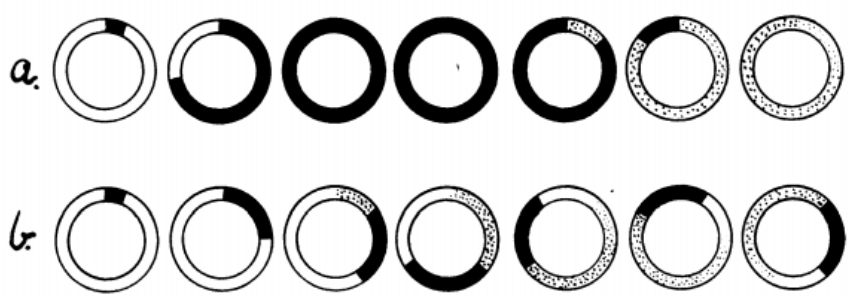

Figure 3: Diagram to show the relation between circuit pathlength and wavelength of excitation and its effect on circus reentry[12]. **(a)** The rate of impulse propagation (solid black) is equal to the duration of the excitation (dotted black) and so by the time the impulse completes one circuit, it cannot propagate any further as the tissue encountered has not recovered from the refractory period. **(b)** The rate of impulse propagation is much slower than the duration of the excitation, or in other words, the wavelength is much shorter than the pathlength (circuit perimeter) and so circus reentry occurs.

The multiple ectopic foci theory was seemingly disproved when Garrey[11] showed that fibrillations ceased when cutting away a small piece of a fibrillating heart, emphasizing the relation between AF sustainability and tissue size. Garrey proposed that it was actually the inhomogeneity, specifically the relative differences in excitability and conductivity between tissues that cause circus motion, not just anatomical blocks.

1.2.2 Experimental Development: Multiple Wavelets and Spiral Waves

Since their proposal, the theories have been experimentally well supported. In 1948, the ectopic foci theory resurfaced when Scherf[13] found that injecting aconitine into the SA node could induce AF and that cooling the injection site stopped the fibrillation instantly.

However, neither the focal ectopic or circus reentry mechanisms, which occur which rhythmicity, were sufficient explanation for the chaotic nature of AF. Moe *et al.*[14] then postulated that the initial wavefront, generated by either mechanism, split into *multiple wavelets* when moving through the inhomogeneous tissue. It is then the interaction of these wavelets, which cause the irregularity in AF.

Allessie *et al.*[15] observed circus motion and multiple wavelets converging centripetally inward around an inexcitable core free from anatomical obstacles. The *leading circle reentry* model was then introduced where the pathlength is now defined by electrophysiological properties of the tissue compared to Mines'[10] model where it was defined by the perimeter of the anatomical obstacle (figure 4).

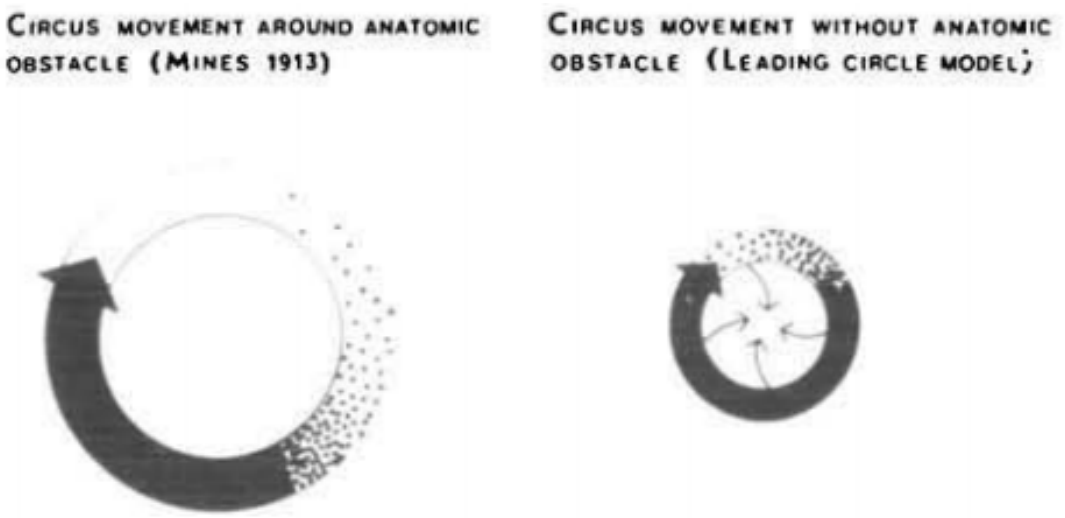

Figure 4: A comparison of circus motion with (Mines 1913) and without (Allessie 1977) the presence of an anatomical obstacle[15]. With an obstacle, the pathlength is defined by perimeter of the obstacle and is such that the front of the circulating wavefront is biting the refractory tail. There may exist a gap of tissue which has recovered from the refractory period and is readily excitable. Without an obstacle, in the Leading Circle model, the pathlength is dependent on the electrophysiological properties of the tissue and the circuit is closed

Spiral waves were described to be waves circulating no anatomical obstacle, generated by rotors with 'vortex-like' activity[16] (figure 5b). Skanes *et al* experimentally linked spiral waves to the spatiotemporal periodicity of the heart[17] and Jalife[18] proposed that it was the rotors with shorter period that were the source of AF and there should exist a gradient of local activation frequency across the myocardium. Jalife suggested that AF is sustained

by the interaction of wavelets generated by a rotor near the Pulmonary-Vein-Left-Atrium (PV-LA) junction - the 'mother rotor' hypothesis and Morillo substantiated this experimentally[19] . However it is not clear if the PV are responsible for generating the action potential or if they provide preferential reentry paths[6].

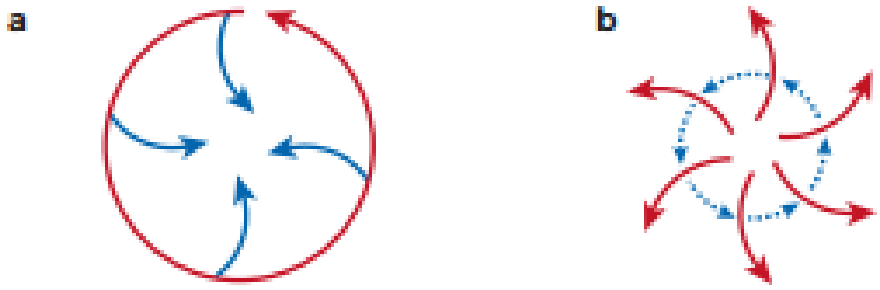

Figure 5: Comparison of Leading Circle Reentry and Spiral Wave[6]. **(a)**) Leading circle reentry model diagram where the pathlength is equal to the wavelength (the product of conduction velocity and refractory period). **(b)** Spiral wave model diagram showing wavelets emanating from an excitable core whereby the persistence of the wavelets is dependent on the angle of curvature and tissue excitability.

1.3 Current Treatment

Treatment of AF today is built upon the limited understanding of the mechanisms of AF discussed above. Radiofrequency ablation of areas of ectopic foci in the pulmonary vein has had a 62% success rate in eliminating AF in patients after discharge[20] whilst the Cox-Maze procedure disrupts the path of the electrical impulse by forming scar tissue on the atrium[21] and has seen more success with long-term cure rates of over 90%[22]. Treatment increasing the refractory period increases the impulse wavelength and therefore the smallest possible pathway too, reducing the number of electrical impulses that can undergo circus reentry[15] . However this theory contradicts clinically effective antiarrhythmic drugs, which decrease the conduction velocity, and therefore the wavelength, which should perpetuate AF instead[23]. But in recent times there has been a shift away from pharmacological treatment as the effects on the electrophysiology of the ventricles can lead to proarrythmia[24] and increase mortality.

No theory has emerged as the sole cause of AF but experimentally it is understood that the mechanism inducing AF is not necessarily the same one maintaining it[14]. It is therefore vital to investigate further the interaction with the atrial tissue in order to gain the adequate insight to increase the effectiveness of AF treatment.

1.4 Modelling Atrial Fibrillation

Major technological advances towards the end of the 20th century allowed the complex excitation interactions of AF to be visually mapped and better understood by computationally modelling them in 2D.

Biophysical models are more detailed and consist of a system of coupled, ordinary differential equations modelling cell membrane's behaviour that must be numerically solved e.g. the Hodgkin-Huxley equations[25] which most biophysical models of excitable cells are based on[26]. Cellular Automata (CA) models approximate the myocardium into a discrete grid and are advantageous over the more biophysically accurate alternative, as they are less computationally demanding to simulate.

Moe *et al.* developed the first significant CA model[27] and found the inhomogeneity of the refractory period sustained the fibrillation and that increasing the refractory period length or reducing the model size was effective in stopping AF. Gerhardt[28] produced the CA model to account for the effects of dispersion and curvature and discovered that the self-reproduction of spiral waves was due to spatial inhomogeneity breaking up the wavefronts (figure 6). Bursting rotors were observed by Bub[29] in embryonic chick heart cells and from the CA model developed it was deduced that the bursting was due to the local interactions of the nonbursting elements. Later, Bub computationally replicated and deduced that it was the heterogeneity of the cells' coupling strength which propagate spiral waves in AF, specifically[30].

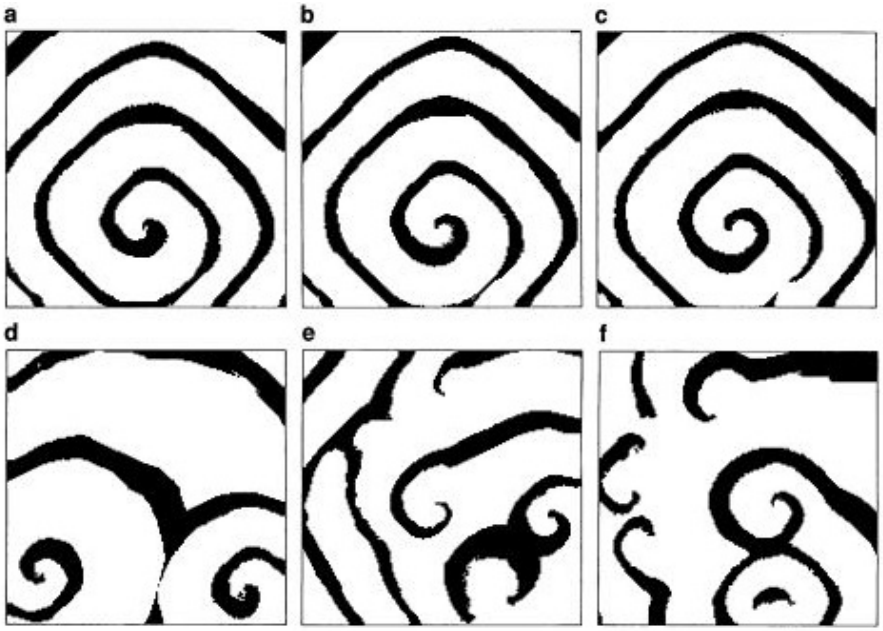

Figure 6: Chaotic self-reproduction of spiral waves by wavefront breakup[28]. **(c)** The original spiral wavefront undergoes breakup at the lower edge, resulting in two counter-rotating spirals in addition to the original rotor. (**d**) The wavefronts of the spirals then interact, multiplying and absorbing simultaneously in an unpredictable cycle.

Qu *et al.*[31] investigated a 2D biophysical model and found that spiral stability was dependent on restitution of action potential duration (APD) and curvature. The development from tachycardia to fibrillation was linked to the transition from a stable spiral core towards a chaotically meandering core.

Most recently, Christensen *et al.*[3] built a CA model to mimic the branched network of the myocardium by using a variable transverse cell-coupling probability and identified the regions critical to initiation and maintenance of AF. Taking a complexity approach, it was found that a critical threshold of the heterogeneity of transversal coupling existed, beyond which AF initiates itself. This threshold value decreases with increasing refractory period as fewer reentry circuits form. A strong link was also implied between AF and fibrosis, which encourages the transversal uncoupling of cells, increasing the heterogeneity. The model also identified the critical regions of AF activity, providing better insight into ablation therapy, once experimentally verified.

Fibrosis is a form of structural remodeling within the heart as the excess collagen deposition separates cells by reducing their coupling, creating a barrier to impulse propagation. These areas result in slowed conduction velocity, increasing the heterogeneity, providing the blocks for reentry to occur[11][4]. However it was implied by Burstein[4] that there may be an upper limit to the relation between fibrosis and AF, and that too much fibrosis can start to terminate AF. On a greater level of complexity, a study conducted by Alonso *et al*[32] suggested that that the inhomogeneity of the cardiac tissue was well represented when the fraction of cell connections was close to the percolation threshold of the lattice as moving from a homogeneous to heterogeneous area of tissue mimics the real case of damaged tissue, (possibly by fibrosis), causing reentry circuits.

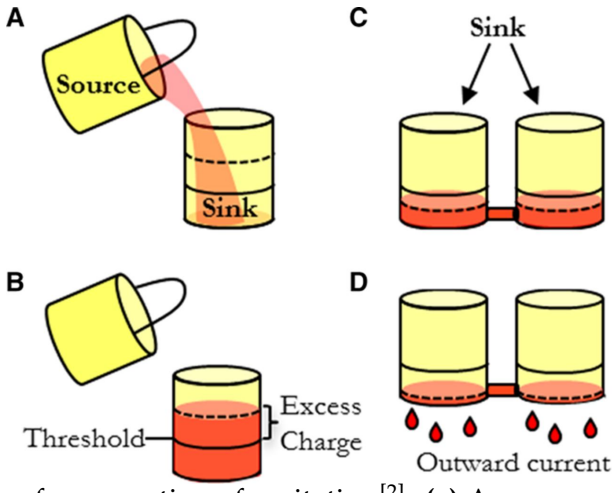

Figure 7: Bucket analogy of propagation of excitation[2]. **(a)** A source passes all its charge to one sink. **(b)** An excitation threshold must be surpassed for the sink to be excited. **(c)** If the source is connected to two cells, the sink size has effectively increased, reducing the rate at which either sink can be filled up to the excitation threshold. **(d)** If the sinks are also connected, they 'leak' charge, effectively increasing the time taken to excite them even further.

Spector[2] investigated the heterogeneity of conduction velocity, specifically looking at its relation to cell connectivity. An excited cell is considered a bucket of source charge and the cell's unexcited neighbours are the sink buckets to which the source charge is poured (figure 7). The *safety factor* is defined as the ratio of charge supplied to a source cell against the charge required to reach its excitation threshold, and any less than 1 and propagation would fail. Therefore as the number of neighbours connected to the source bucket increases, the sink size increases. This reduces the safety factor, taking longer to fill up each single sink bucket, thereby reducing overall conduction velocity.

1.5 Moving Forward

There exist several theories for the initiation and maintenance of AF, but whilst new theories have emerged with time, there is still no clear winner. It may be suffice to accept that AF is induced and maintained by different mechanisms, but it would appear that, whether it be the refractory period[27], cell coupling[3][32] or conduction velocity[2], it is the heterogeneity of the myocardium that is key in perpetuating if not also initiating AF. Using a complexity approach, a simple model of the heart can be used to identify the critical structural features that emerge within the myocardium responsible for causing and maintaining AF. It is therefore insightful that the model by Christensen *et al.* be further developed to incorporate more layers of heterogeneity across the heart and faithfully mimic the heart in all its complexity.

2 Theory of the Cellular Automata Model

2.1 Christensen *et al*'s Original Model

The original cellular automata model as defined by Christensen *et al*[3] uses a simple square lattice of $L \times L$ cells to discretize the propagation of excitation waves throughout the heart tissue. The states of each cell are updated with every time step as a cell instantaneously transfers all its excitation charge to its connected neighbours.

The model overlooks sub-cellular processes and simplifies the complexity of the heart's behaviour, allowing analytical calculations to be made. There is a set of rules by which the model follows to accurately mimic the heart. A set of pacemaker cells exists on the left-most column of the lattice, which generates excitation impulses with a frequency equivalent to the Sino-Atrial Period (SAP). All cells are horizontally coupled such that this wavefront can propagate left to right and a cell's state is dependent on its four nearest neighbours.

A fraction of the cells (ν) form a vertical couple to mimic the branched network of cardiomyocytes. The length of the couples is negligible in comparison to the cells and therefore does not affect the overall dimensions of the model. A fraction of the cells (δ) are defective and so if any of their excited neighbours attempt to excite them, there is a chance of ϵ that they will not excite and remain in a resting state, representative of electrical dysfunction in the myocardium.

Parameter	Description	Value
L	**Length** - Number of cells in one direction of the lattice (model is a 2D lattice)	200
τ	**Refractory Period** - Period of inexcitability that an cell goes into after excitation	50
SAP	**Sino-Atrial Period** - Frequency of pacemaker-generated excitation impulses	220
δ	Probability of a cell being **defective**	0.05
ϵ	Probability of a defective cell **misfiring**	0.05
ν	Probability of a cell having **one vertical coupling**	0.14 (critical)

Table 1: Parameters within the CA model

In addition to the pacemaker cells, periodic boundary conditions exist that top and bottom row are connected, forming a hollow cylinder of circumference and length both equal to L. The parameters are summarised in table 1 with the numerical values assigned to them in the model.

Every cell starts off in a resting state but following a pacemaker-generated impulse, can become excited, and in the following timestep, excite their connected neighbours too. The excited cells themselves go into a refractory state in the next timestep where they cannot be excited by any of their connected neighbours for a duration of τ timesteps.

1. At time step t:
   - A cell (i) excites if any of its connected neighbours were excited at timestep $t-1$
2. At time step $t+1$:
   - Any resting, connected neighbours of cell i become excited
   - Cell i goes into refractory state for $-\tau$ timesteps
3. At time step $t+2$:
   - Any resting, connected neighbours of connected neighbours of cell i become excited
   - Excited, connected neighbours of cell i go into refractory state for $-\tau$ timesteps
   - Cell i remains in a refractory state for another $-\tau+1$ timesteps

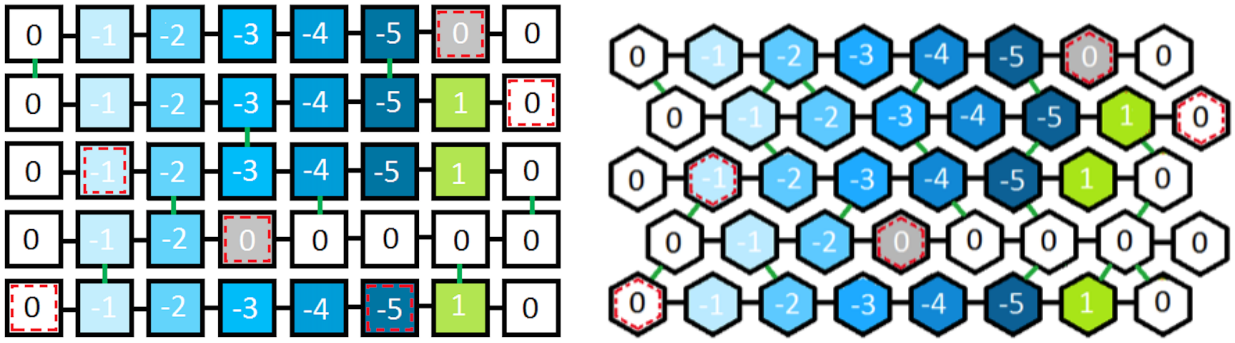

(a) Square Model **(b)** Hexagonal Model

Figure 8: An excitation wave passing through a square and the hexagonal counterpart is shown. The excited cells are green whilst various shades of blue represent different stages of the refractory period. The defective cells are outlined in red and those that failed to excite are grey. Numerically, resting cells $= 0$, excited $= 1$ and refractory state takes values incrementing from $-\tau$ all the way up to 0, where the cell returns to its default resting state. For this example, $\tau = 5$.

2.2 Hexagonal Model

Utilising the definition of the original model in the previous section as a stepping stone, a new model was built from scratch to further investigate the critical structural features that emerge within the myocardium as a result of its heterogeneity.

The original model simplified the connectivity of the cells, limiting the number of vertical connections in either upward or downward direction to only one. In real cardiac tissue, cells form a branched network with a high degree of randomized vertical interconnection. They are not homogeneously laid out in a square lattice and therefore a more realistic representation would be to use a hexagonal lattice and maintain the parameter ν as the probability of a cell forming one vertical couple, where the maximum possible vertical couples a cell can form has increased from 2 to 4 (figure 9).

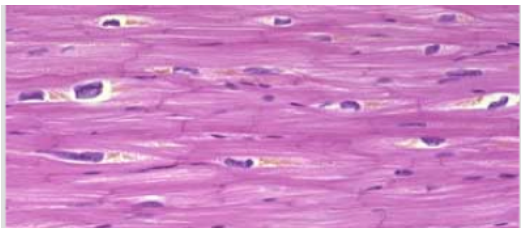

(a) Real cardiac tissue is branched [33]

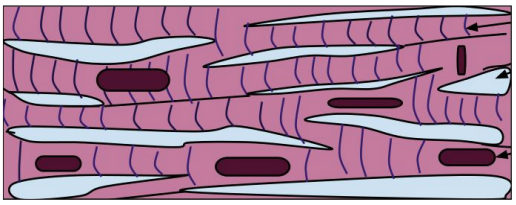

(b) Close up of the branched network [34]

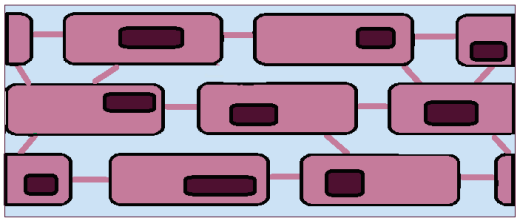

(c) Brick layout representation

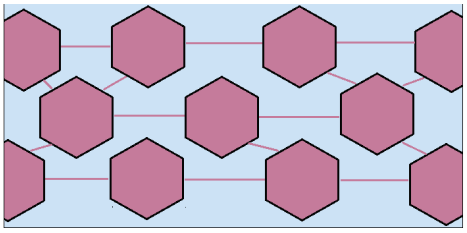

(d) Hexagonal lattice representation

Figure 9: (a) Real cardiac cells appear branched. **(b)** The cells have more than one vertical coupling per cell. **(c)** They can be visualised as discrete cells in a brick layout where two vertical couples can form in either upward or downward direction. **(d)** This can be represented using a hexagonal lattice.

2.3 Risk of Atrial Fibrillation

The cause of AF has widely been attributed to the formation of rotors, which are re-entering circuits of excitation [10] [11] [15] [16] [18]. The wavelength (λ) is the minimum path length a rotor can take and is defined as

$$\text{Wavelength}(\lambda) = \text{Conduction Velocity (CV)} \times \text{Refractory Period}\,(\tau) \tag{1}$$

A rotor can sustain when the pathlength taken by a reentry circuit is greater than λ, allowing the cells along the path to have recovered from their refractory state and be reexcited by the re-entering wavefront. The underlying structure of the model, based upon the density of defective and vertically coupled cells is responsible for the rotor formation.

The simplest form of a rotor (figure 10) exists over only two neighbouring rows of the lattice and utilising equation 1, forms when the distance from a defective cell to the next vertically coupled cell (l_i) satisfies

$$(l_i) > \frac{\tau}{2} \tag{2}$$

This condition is defined as being critical as there is a chance the defective cell misfires and blocks the wavefront, leaving the cells further along along that row unexcited. If a vertically coupled cell exists at least $\frac{\tau}{2}$ cells away from the original defective cell, then a simple rotor can form and sustain itself until that defective cell misfires again.

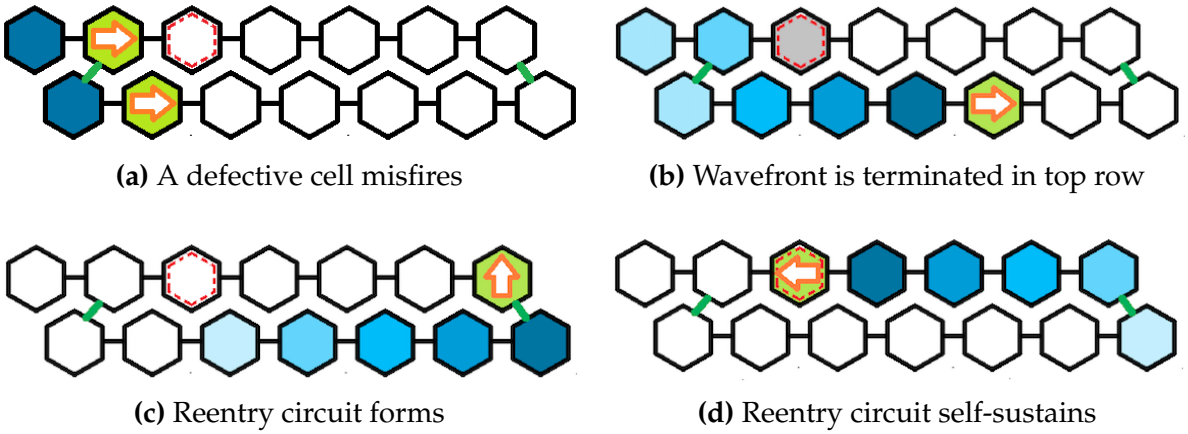

(a) A defective cell misfires

(b) Wavefront is terminated in top row

(c) Reentry circuit forms

(d) Reentry circuit self-sustains

Figure 10: Formation of a simple reentry circuit within a hexagonal lattice. Green cells are excited and blue cells are refractory. Defective cells are outlined in red and the grey cells represents a defective cell misfiring. **(b)** The wavefront is blocked along the top row by a misfiring defective cell but continues to propagate along the bottom row. **(c)** Upon reaching a vertically connected cell at a distance greater than $\frac{\tau}{2}$ away from the defective cell, the wave front reenters. **(d)** It propagates back along the top row, provided the defective cell does not misfire again, forming a self-sustaining circuit.

The probability that there exists at least one defective cell in the entire lattice that is critical is then defined as the probability of the hexagonal lattice being at risk of AF (P_{risk}).

$$P_{risk} = 1 - [1 - (1 - \nu)^{2\tau}]^{\delta L^2} \tag{3}$$

See appendix A for full derivation of P_{risk} based upon the derivation for the original square lattice[3].

2.4 Heterogeneous Conduction Velocity

2.4.1 Timedelay (Δt)

So far the conduction velocity of the excitation wavefront (CV) has been uniform across the lattice. This is not representative of the heart's behaviour, which relates the connectivity of the lattice to the propagation speed[2], yielding instead, a heterogeneous wavefront. The aim was to incorporate the source sink notion[2] into the existing model and let the number of connections a cell had, dictate the CV of excitation charge through that cell.

Connected neighbours of the excited cell will also have their own connected neighbours and realistically will be continuously leaking excitation charge out as they receive, slowing down the CV even further. However it is difficult to discern the cutoff range of connected neighbours that should affect a given excited cell. Therefore it is suffice to represent the behaviour of heterogeneous CV in the model using a discretised simplification where only the immediate connected neighbours of the excited cell are considered. Using the bucket analogy[2] (figure 7), this means that the number of sink buckets receiving water from the source bucket is a factor, but whether or not the sink buckets are leaking, is not.

A new parameter and state called timedelay (Δt) was defined to represent the behaviour that a more coupled cell has slower CV.

$$\Delta t = \frac{1}{CV} \tag{4}$$

$$\Delta t = \text{Number of Cell Connections} - 1 \tag{5}$$

The offset of -1 in equation 5 is required as all cells have at least 2 horizontal couples by default as defined by the original model and so these cells, which essentially have no vertical couples, must still propagate at the original homogeneous speed.

Equations 4 and 5 state that Δt is greater for cells with more connections (a maximum of 6 in a hexagonal lattice), mimicking the behaviour that the more buckets a source must fill, the slower it takes to fill each one up.

Implementing timedelay means that when a cell is excited, it goes into a timedelay state for a period of $\Delta t - 1$ timesteps, decreasing its state by 1 with every timestep until it reaches 1 and is in the excited state. If a cell has $\Delta t = 1$ (no vertical coupling), it will excite immediately as before (figure 11).

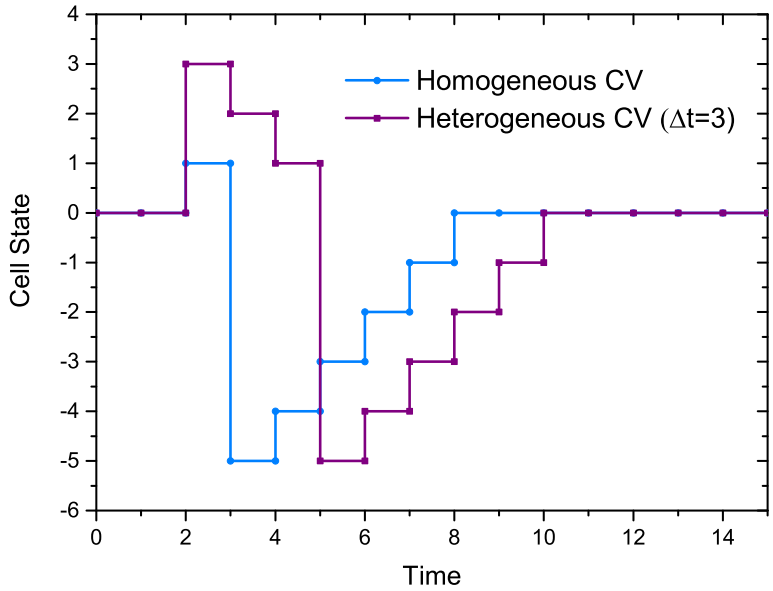

Figure 11: A comparison of the states of a cell with $\Delta t = 3$, following excitation is shown for both homogeneous (blue) and heterogeneous (purple) CV. Both cells are 'excited' at $t = 2$, but the heterogeneous model goes into a timedelay state for a duration of $t = \Delta t - 1$ before being the cell's state is actually excited (equal to 1) at $t = 4$. For both models, τ is set to 5 in this example.

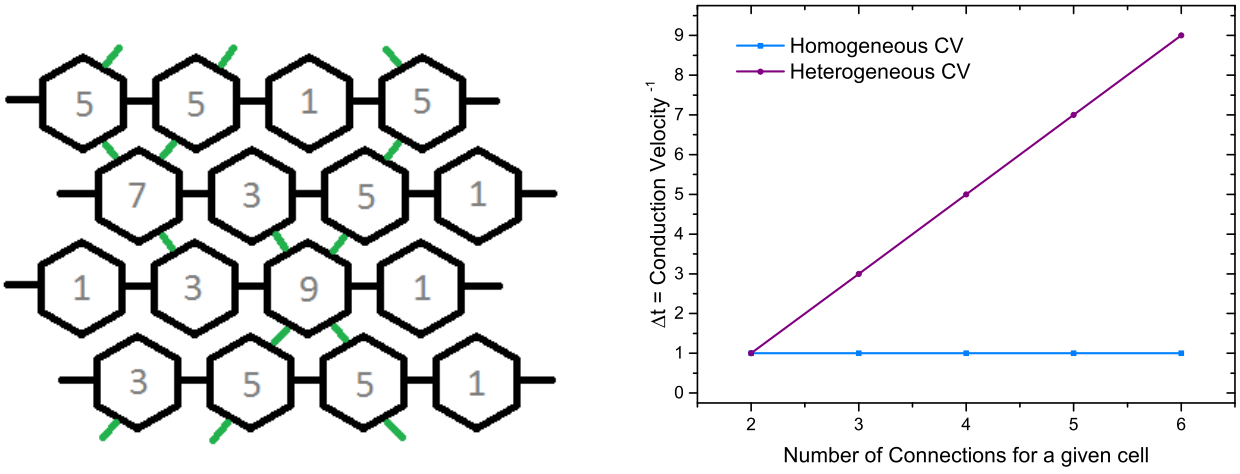

(a) **(b)**

Figure 12: A comparison of timedelay (Δt) in a heterogeneous CV model against the original homogeneous CV model. **(a)** The exaggerated timedelay is assigned given the connectivity of a lattice using equation 6. As seen, a cell with 6 connections has $\Delta t = 9$ whilst a cell with no vertical connections has $\Delta t = 1$. **(b)** The difference in CV for a given cell is represented for both homogeneous (blue) where CV is uniform and heterogenous (purple) where it is dependent on the number of connections that cell has, given by equation 6.

2.4.2 Exaggerating Timedelay (Δt)

The relation for timedelay and cell connectivity described in equations 4 and 5 was increased linearly by a factor of 2 to noticeably exaggerate the observed effect upon the hexagonal model of a heterogeneous CV using equation 6 (figure 12b).

$$\Delta t_{exag} = 2 \times \text{Number of Cell Connections} - 3 \tag{6}$$

Another offset of -3 was required so that cells with only 2 horizontal (or no vertical) connections still returned a timedelay $\Delta t = 1$. A maximum $\Delta t = 9$ now corresponds to a cell having a maximum of 6 connections (figure 12a). For the remainder of the report, timedelay (Δt) refers to the exaggerated expression obtained in equation 6.

2.5 Patch

Atrial fibrosis is the formation of excess collagen (scar tissue) within the myocardium, reducing local intercellular connectivity, effectively lowering ν for the local region[?]. It was of interest to mimic these conditions throughout the heart to see how regions of lower connectivity can affect the risk of AF.

A patch was defined in the centre of the lattice of a set radius and the cells chosen to be within the patch were set to a lower value of ν (ν_{local}) in a naive attempt to replicate the effects of fibrosis by reducing cellular connectivity.

2.5.1 Percolation

The previously mentioned patch is a very basic representation of the behaviour of fibrosis and so another patch was defined to examine fibrosis with greater complexity. Instead of setting the entire patch to a lower ν, the intercellular connectivity was reduced down to the percolation threshold[32] (such that the wavefront just about propagates across the patch). This is because fibrosis is the gradual loss of cellular connectivity over time[?], and so it was more realistic to remove links from a patch which was originally 'healthy', having the same connectivity as the rest of the lattice. A horizontal bias in patch connectivity was set such that a wavefront still effectively propagated from left to right across the lattice.

The process for finding the critical percolation threshold with horizontal bias:

1. Set up a patch with $\nu_{local} = \nu$. By definition, this patch is 'percolating' and the couples are already horizontally biased as all horizontal links are present by default whilst vertical links are set by ν.
2. Remove a fraction of all links randomly (vertical and horizontal equally).
3. Check if remaining connections percolate across patch.
4. Keep removing links until connections no longer percolate.
5. Return the last set of removed links such that patch is at the percolation threshold.

3 Method and Implementation

The models outlined above were implemented using C++ (see appendix C for the code).

3.1 Boundary Conditions

The hexagonal model utilises the same boundary conditions as the original model in that the top and bottom rows are connected. The left-most column forms the pacemaker cells which never be defective so that a pacemaker generated impulse of L cells is sent out without fail. The final column of cells have no right horizontal couple such that the wave of excitation stops propagating outside the lattice.

However moving over to a hexagonal lattice raises other boundary issues. In order for the hexagons to tesselate, the columns of the hexagonal lattice do not align. Instead, the odd and even rows are out of alignment with each other (figure 13a). This creates a problem for cells in the last column as, whilst the last column cells in an even row can form both a right upward and downward connection, the odd row cells cannot (figure 13b). Therefore it was important to address these boundary issues in the computational model in order for it to work as desired. For a lattice of size L, L must be an even number such that the top and bottom row are of different parity and can tesselate, mimicking a hollow cylinder structure.

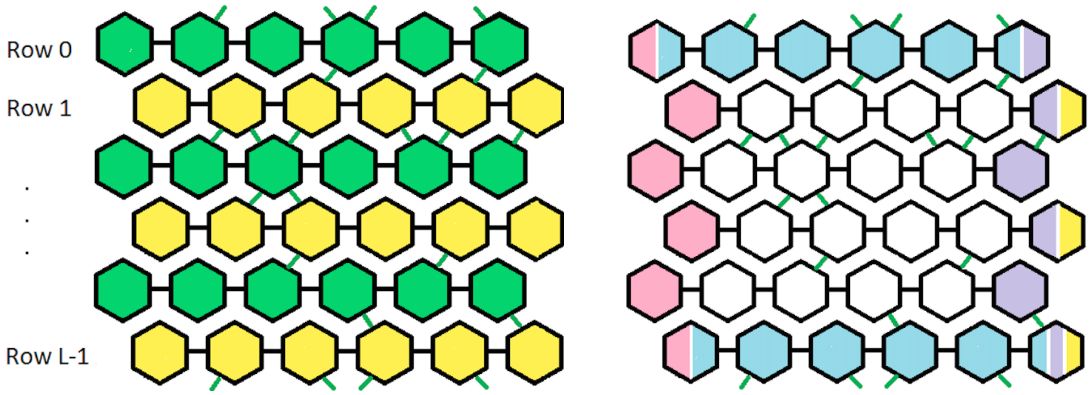

(a) Odd and even rows are out of alignment

(b) All the cells where boundary conditions apply

Figure 13: The boundary conditions are shown for a hexagonal lattice of $L \times L$ cells where L must be an even number to uphold the conditions. **(a)** It is seen that the odd (yellow) rows are out of alignment with the even (green) in order for tessellation to occur and that no right neighbours exist for cells in the last column to couple to. **(b)** Pacemaker cells (pink) are defect-free, top and bottom row cells (blue) can vertically couple to each other. Last column cells (lilac) have no right horizontal couple such that the excitation wave cannot travel any further than the lattice, and the odd row cells in the last column (yellow) cannot have any (horizontal or vertical) right couplings at all.

3.2 Algorithm Structure

A Mersenne Twister random number generator was used to randomly distribute the defects and connectivity using the parameters in Table 1. Horizontal couples are formed in a rightward direction whilst vertical couples are in a downward direction (figure 14). This is to ensure that double couples do not form in the case where a cell is randomly selected to form a couple with its neighbour and then that neighbour is itself selected later. Although there is no effect upon the model, this problem was addressed with the purpose of having an efficient code.

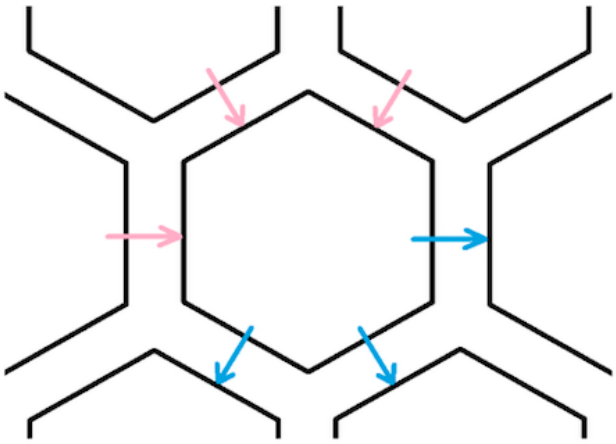

Figure 14: The direction of coupling in the model is outlined. The blue couples represent the couples that have formed as a result of the cell being randomly chosen whilst the pink couples represent the couples that the cell's neighbours are responsible for.

For each simulation, the model is initialized using a new seed for the random number generator using the following steps:

1. $L \times L$ cells are created in a resting state.
2. The timedelay (Δt) of all cells is set to 1.
3. All cells, excluding any in the last column, form a **rightward horizontal** connection.
4. A random selection of cells, excluding the pacemaker cells, are declared **defective**.
5. Another random selection of cells are chosen to form a **left downward vertical** connection. The timedelay of these cells and the cells that they connect to are incremented by 1.
6. Step 5 is repeated for the **right downward** connections.
7. The timedelay of all cells is exaggerated using equation 6.
8. The pacemaker cells are excited, ready to initiate a wavefront throughout the rest of the lattice.

The model then runs through the time loop just as in the original square model, the key difference being that instead of immediately taking the excited state of 1, a resting cell takes on its timedelay value when excited (figure 15). It subsequently decreases its state by 1 in every following timestep until it reaches 1 and can become excited. In the case where a cell's timedelay $= 1$ then it excites immediately as before.

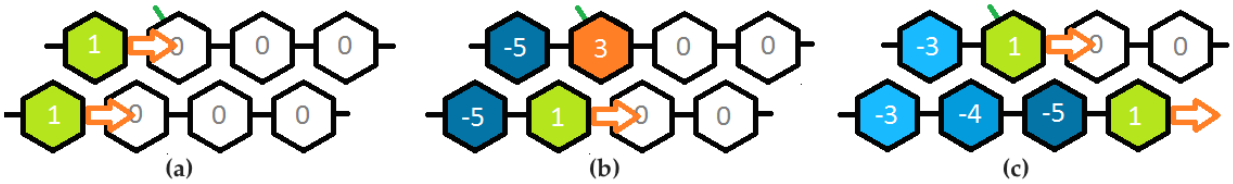

Figure 15: (a) An incoming excitation wave front is slowed down in the top row by the cell with a vertical couple meaning it has a greater $\Delta t = 2$ and cannot excite immediately. **(b)** It goes into a timedelay state for a period of 2 timesteps before it can reach the excited state. **(c)** As a result, heterogeneous CV is observed as the wavefront in the top row is now behind that in the bottom row.

3.2.1 Efficiency

To increase the speed of the model certain checks were employed to ensure maximum efficiency.

In every timestep, the state of every cell in the lattice is updated to simulate the spread of the excitation. For a non-fibrillating model, as $L < SAP$ and only one pacemaker-generated wavefront can exist on the lattice at a given time. The approximation can be made that there exists L excited or time-delayed cells and $L \times \tau$ refractory cells. The remainder of the lattice remains in a resting state until the wavefront reaches them, making it a waste of time to keep scanning through the entire lattice to update every cell.

Therefore for every time step, instead of updating the entire lattice, the model only scans through the lattice for cells which are not resting and updates them and their connected neighbours. This check means that during non-fibrillation, more than half the lattice is bypassed, speeding up the model's performance time.

Another feature was to prevent a defective cell, which has a chance of misfiring, from being excited multiple times within one timestep if it has more than one excited neighbour. This was achieved by tagging a cell once a neighbour had attempted to excite it so that only untagged cells could attempt to be excited. The tags were cleared for every timestep.

3.2.2 Detecting AF

When running the model, the definition of the model being 'fibrillatory' was defined as the lattice having more than $1.2L$ excited cells at any given time. This accounts for the pacemaker-generated wavefront, defective cells misfiring and reentering circuits that do not sustain as they do not fulfill equation 2. Once the number of excited cells in the system exceeds this limit, the system is labelled as 'fibrillatory' and a numerical definition of the system being at risk of AF can be defined as

$$P_{risk} = \frac{\text{Timesteps in AF}}{\text{Total Timesteps}(t_{max})} \tag{7}$$

The numerical data can be compared to the analytic expression (equation 3) to verify the model is working.

3.3 Statistics

The results obtained in the results section were all averaged over $S = 50$ simulations per data point where each simulation used a different seed for the random number generator and each simulation lasted a $t_{max} = 10^6$ timesteps. Error bars are shown wherever data is collected numerically (see appendix C for handling).

3.3.1 Heterogeneous CV scaling

As ν increases and more vertical couples exist in a lattice, the average timedelay of the lattice ($\langle \Delta t \rangle$) is increased too. This reduces the average CV of a wavefront (equation 4) in the Heterogeneous CV model such that it takes longer for one wavefront to propagate through the lattice so that multiple wavefronts can be present on a non-fibrillating lattice. Therefore SAP and t_{max} had to be scaled up by $\langle \Delta t \rangle$ too in order to address the slower CV.

However for $\nu = 1$, $\langle \Delta t \rangle = 9$ and scaling up would mean a total timesteps of $t_{max} = 9 \times 10^6$ which is an impractically long duration, so in order to accommodate $\langle \Delta t \rangle$ scaling, t_{max} was to be reduced to a default of 10^5 before scaling for the Heterogeneous CV model.

3.3.2 Ignoring transient state

The lattice can either be in a transient or recurrent state. Whilst transient states occur at most once, after a cross-over time the lattice stabilises and becomes recurrent. When $t_{max} = 10^6$, the period of time spent in the transient state was insignificant, however for the Heterogeneous CV model, where t_{max} is reduced to 10^5, this transient period has greater influence. A discount time was defined as $40 \times SAP$ so that results were not collected from the lattice whilst it was still in its transient state so that the data for heterogeneous CV was not skewed as a result of t_{max} being smaller.

4 Results and Discussion

4.1 Homogeneous Conduction Velocity

4.1.1 Comparison to Original Square model

As our model was built from scratch, the first aim was to see if it could reproduce the results of the original square model and verify that it was performing simulations correctly. The model was set using the parameters in table 1, but with ν (vertical coupling probability) varying from 0 to 1. The numerical P_{risk} was recorded using equation 7 and plotted against the analytical expression for a square lattice (appendix A, equation 27).

The numerical data obtained fits the analytical expression well, verifying the algorithm. The model was then set to its hexagonal state and the same data taken but instead using equation 3 for the hexagonal analytical values. The analytical and numerical results are displayed for both the Original Square and Hexagonal models in figure 16.

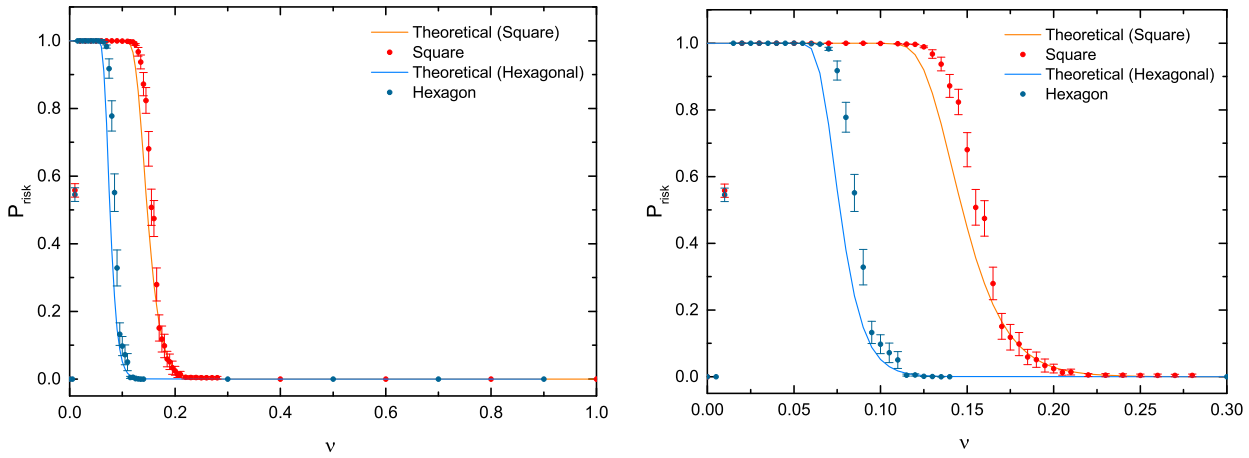

(a) Results for full range of $\nu = 0$ to 1

(b) Zoom in where P_{risk} is non-zero

Figure 16: The numerical (dots) and analytical (line) P_{risk} for both the Original Square (red) and Hexagonal Homogeneous CV (blue) models are shown against ν using parameters outlined in table 1. A critical value is observed at $\nu = 0.14$ and $\nu = 0.07$ for the Square and Hexagonal models respectively. From this point, the risk rapidly increases as ν decreases. This is the point at which the lattices have become critically connected such that equation 1 and 2 are fulfilled making rotors much more likely to form and AF is able to sustain itself.

Vertical coupling is crucial for AF to induce, if no vertical couplings exist then there is no vertical path for a wavefront to reenter and form a rotor. However, the more vertically coupled a lattice becomes, the more likely it is that the next vertically coupled cell is closer to the defective cell than the minimum distance (l_i), meaning it is more unlikely that the conditions expressed by equations 1 and 2 can be fulfilled. Therefore there exists a critical

value for vertical coupling ν_{crit} above which AF no longer sustains in the lattice. The behaviour of the model as ν decreases from 1 to 0 is reminiscent of the real behaviour of AF which transitions from being non-fibrillatory ($\nu_{crit} < \nu$) to paroxysmal ($\nu \approx \nu_{crit}$) to finally persistent AF ($\nu < \nu_{crit}$) (figure 17).

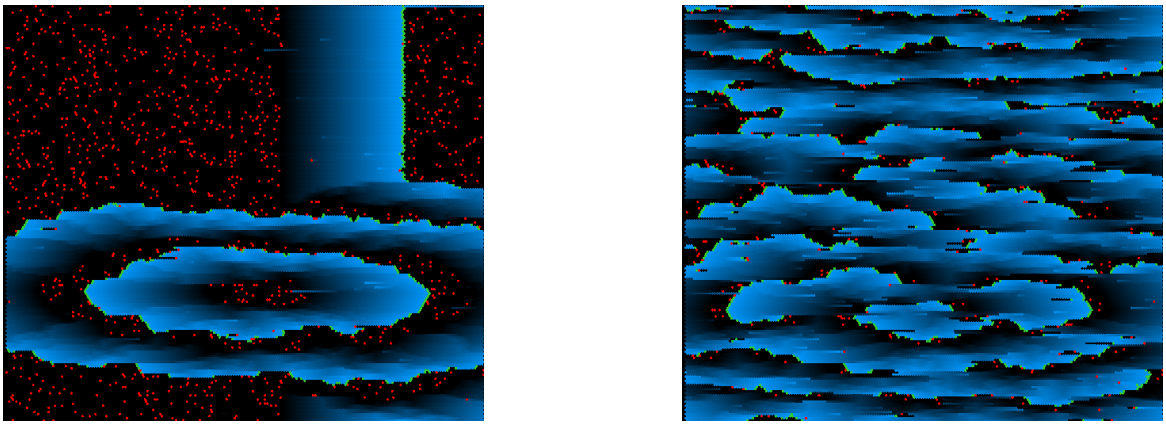

(a) Paroxysmal AF at $t = 2377$ **(b)** Persistent AF at $t = 50173$

Figure 17: Corresponding screenshots to show paroxysmal and persistent AF within a Hexagonal Homogeneous CV model for $\nu = 0.07$. Red cells are defective, green cells are the excited wavefront and varying shades blue are the refractory state cells. **(a)** A single rotor forms and self-terminates. **(b)** Several rotors form over the lattice and sustain long enough for their wavefronts to interfere and induce persistent AF.

The critical value of ν is the steepest point on the analytic curve, and has reduced from around 0.14 to 0.07 (figure 16) as the model shifts from a square to a hexagonal lattice, indicating a lower likelihood of AF in a hexagonal lattice. It is expected that in a hexagonal lattice, where each cell is twice as likely to be vertically coupled compared to the original square lattice, that the risk of AF be twice as *less* likely.

The results outlined in the rest of this report are from the model being in a hexagonal lattice.

4.2 Heterogeneous Conduction Velocity

Recall that by introducing a timedelay state, cells with any vertical connections will not go into an excited state immediately after being excited, but instead go into the timedelay state for a period corresponding to the number of vertical connections that cell has (equation 6). The P_{risk} was obtained from the model with Heterogeneous CV implemented using the same parameters as for the Homogeneous model (figure 18).

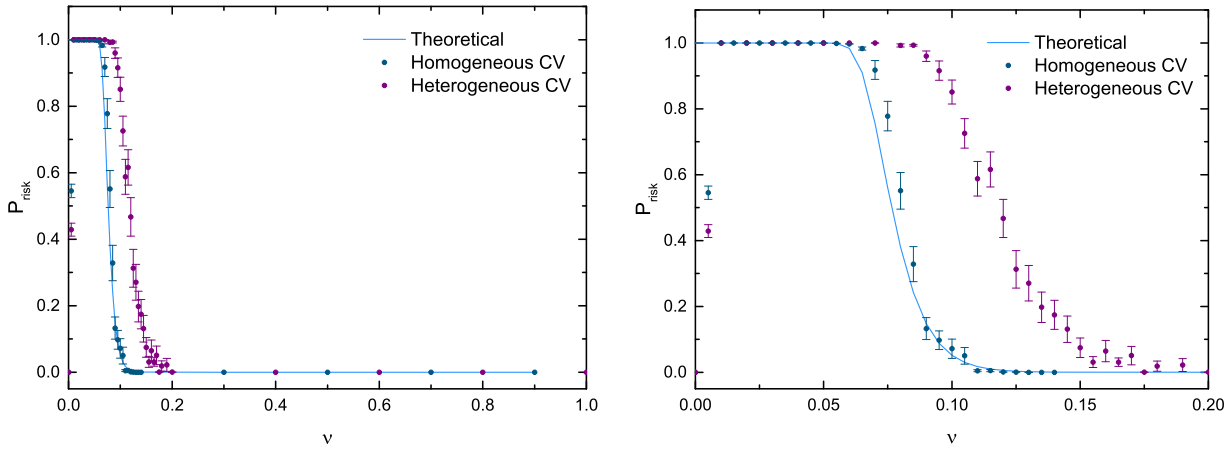

(a) Results for full range of $\nu = 0$ to 1.

(b) Zoom in to where P_{risk} is non-zero.

Figure 18: The numerical (dots) P_{risk} for both the Homogeneous (blue) and Heterogeneous CV (purple) hexagonal models against ν are shown using the parameters outlined in table 1. The analytical P_{risk} for homogeneous is shown (blue line) for reference. There is a clear increase in P_{risk} for all ν when Heterogeneous CV is implemented. The CV of the wavefront has slowed which decreases the minimum pathlength required for reentry for all ν except $\nu = 0$, according to equation 1, thereby increasing the risk of rotor formation and P_{risk}.

The timedelay for the Heterogeneous CV model must now be expressed as an average over the lattice. It has also increased compared to the Homogeneous CV model where CV$= 1$ for all cells in a given lattice.

$$\Delta t_{hom} < \langle \Delta t_{het} \rangle \tag{8}$$

By rewriting equation 1 using equation 4, the minimum pathlength, or the wavelength (λ) of a rotor can be expressed in terms of timedelay

$$\lambda = \frac{\tau}{\Delta t} \tag{9}$$

Using equation 9, the expression in equation 8 comparing the Homogeneous and Heterogeneous CV models can be rewritten in terms of the wavelength

$$\lambda_{hom} > \langle \lambda_{het} \rangle \tag{10}$$

Therefore, for a Heterogeneous CV model, as CV is expected to decrease for all values of ν (except when $\nu = 0$, as no vertical couples exist), the wavefront takes longer to pass from cell to cell. This decreases the wavelength required for AF and fewer cells are required to form a rotor. Therefore for a given ν, AF is expected to be more likely with a heterogeneous wave front.

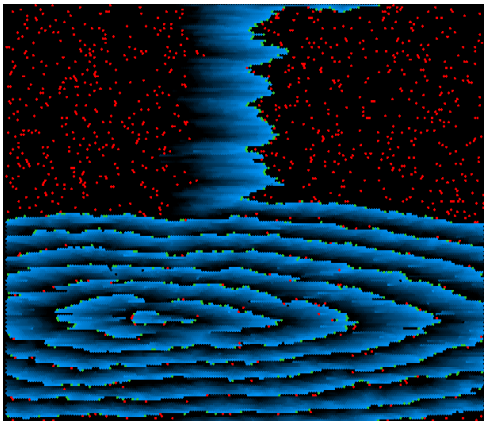

(a) A single rotor initiates AF at $t = 1361$.

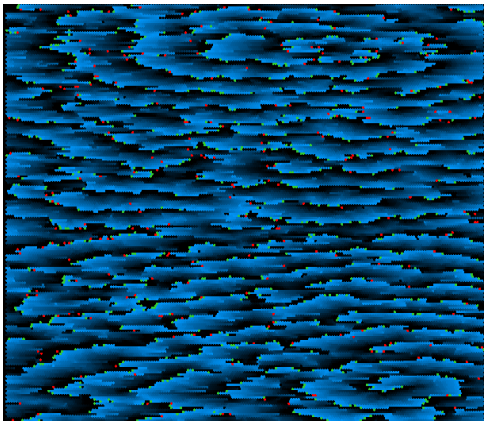

(b) Persistent AF at $t = 50001$

Figure 19: Corresponding screenshots to show the onset of persistent AF within a Heterogeneous CV model for $\nu = 0.1$. Note how the wavefront is now heterogenous and jagged as a result of CV being dependent on a cell's connectivity. The spiral rotors formed are also tighter as the wavelength has effectively decreased compared to the rotors seen for the homogeneous CV model (figure 17).

4.2.1 Finding minimum path length ($\langle\lambda_{het}\rangle$)

In order to quantify the behaviour of the Heterogeneous CV model, the task was set to find the analytical fit for the numerical P_{risk} using the existing analytical expression for Homogeneous CV P_{risk} (equation 3).

Upon inspection, the analytic expression for the Homogeneous P_{risk} is dependent on τ. This is because the expression essentially defines the probability that a vertically connected cell exists at a distance of λ away from a given defective cell, in order for AF to be possible (see appendix A for full derivation). In the Homogeneous CV model, as CV$= 1$ for all cells in the lattice for all ν, using equation 1, the minimum pathlength (λ_{hom}) is therefore simply equal to τ.

For the Heterogeneous model, as CV no longer equals 1 for all cells, the minimum path length $\langle\lambda_{het}\rangle$ is now less than τ and averaged over an entire lattice. Therefore P_{risk} (equation 3) is no longer dependent on τ, but the unknown $\langle\lambda_{het}\rangle$. The next investigation was to find $\langle\lambda_{het}\rangle$ to obtain an analytical fit to the numerical data obtained for a Heterogeneous CV model.

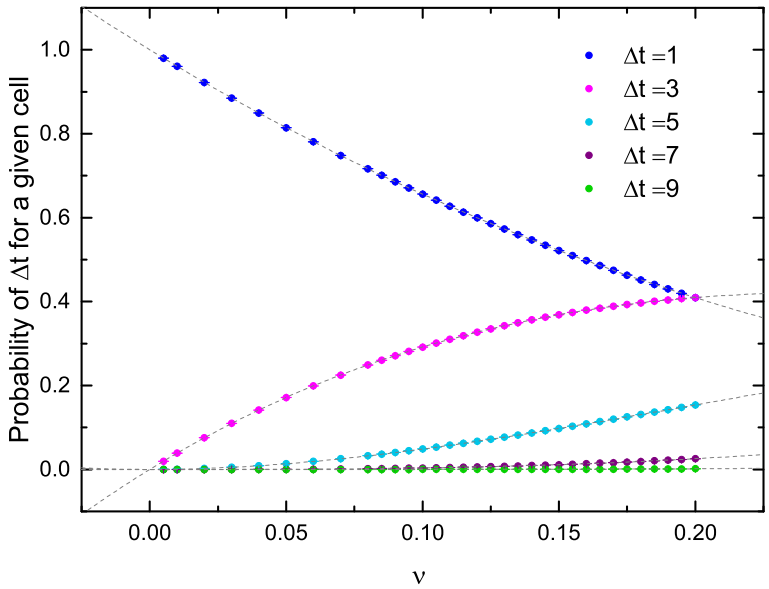

Figure 20: Numerical distribution of cell coupling, and therefore Δt, (dots) ($0 \leq \nu \leq 0.2$ shown here) across a lattice fits a binomial distribution (dashed line).

Recall that Δt is related to cell coupling (equation 6), and the distribution of the vertical coupling within a Heterogeneous CV lattice is binomial (figure 20).

$$P(\Delta t_{i,\nu}) = \binom{n}{r} \nu^r (1-\nu)^{n-r} \tag{11}$$

The number of vertical couples per cell and the number of possible couple arrangements on the cell are given by n and r respectively.

Using the binomial distribution (equation 11) of timedelay for a cell (Δt), the expected timedelay ($\langle \Delta t \rangle$) over an entire lattice can be obtained for a given ν, ($\langle \Delta t_\nu \rangle$).

$$\langle \Delta t_\nu \rangle = \sum_{i=1}^{5} \Delta t_{i,\nu} \cdot P(\Delta t_{i,\nu}) \tag{12}$$

The expected timedelay for a given ν ($\langle \Delta t_\nu \rangle$) can then be input into equation 9 to obtain an expected wavelength for a given ν, ($\langle \Delta \lambda_{het,\nu} \rangle$).

$$\langle \Delta \lambda_{het,\nu} \rangle = \frac{\tau}{\langle \Delta t_\nu \rangle} \tag{13}$$

Replacing τ with $\langle \Delta \lambda_{het,\nu} \rangle$ in the Homogeneous analytical expression for P_{risk} (equation 3) yields an estimation of the analytical P_{risk} for the Heterogeneous CV model, where the wavelength is now dependent on ν (figure 21).

$$P_{risk,het,\nu} = 1 - [1 - (1-\nu)^{2\langle \Delta \lambda_{het,\nu} \rangle}]^{\delta L^2} \tag{14}$$

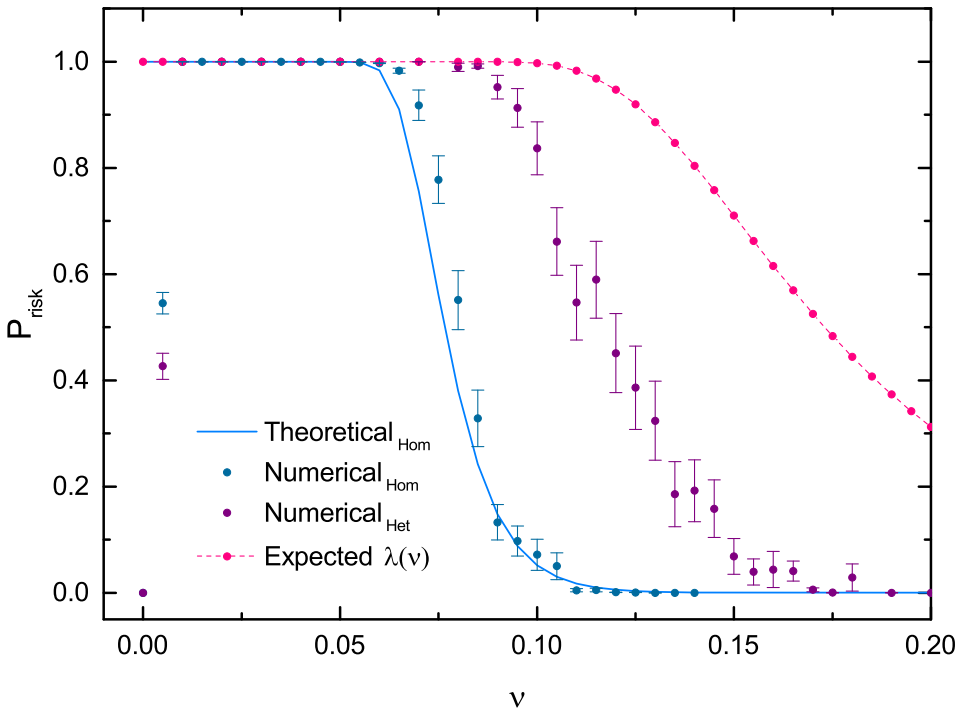

Figure 21: The analytical fit (pink) obtained using expected wavelength ($\langle \Delta\lambda_{het,\nu} \rangle$) using equation 14, is shown against the numerical data (purple). The analytical fit appears to fit the numerical data well up to around ν_{crit}, where the fit starts to deviate from the numerical data, with the deviation become greater as ν increases. The analytical and numerical data for the Homogeneous model (blue) are presented for comparison and some deviation is expected at the critical range, but the Heterogeneous analytical P_{risk} obtained is clearly an overestimate for ν greater than ν_{crit}.

This method yielded a relatively bad fit to the numerical data, in comparison to the analytical fit for Homogeneous CV (figure 21). The analytical expression fits the data up to ν_{crit} where the analytical P_{risk} becomes greatly overestimated. Further investigation into the behaviour of the model around this range was then carried out.

4.2.2 Extremal Statistics

A more thorough look at what is physically going on in the lattice is required to understand where the analytical fit has gone wrong.

A more connected lattice (greater ν), has greater Δt and therefore a smaller wavelength (λ). Based upon this argument and using equation 13, AF risk should still be possible for $\nu = 1$ where $\langle \lambda_{het,\nu} \rangle = 5.56$, indicating that AF, although much less likely to occur, is still possible for a fully connected lattice. In reality, an excitation wave will reenter immediately, never reaching $\langle \lambda_{het,\nu} \rangle$ so there is no possibility of the condition for AF outlined in equation 2 being fulfilled for $\nu = 1$.

This suggests that as the connectivity of a lattice increases (greater ν), the possibility of critical regions forming that can propagate a wavefront at the wavelength is diminished along with the impact of the wavelength upon AF formation.

Therefore, for $\nu_{crit} < \nu$, when measuring P_{risk}, it is more important to consider the connectivity of the lattice as opposed to the wavelength. Wavelength is a result of cell connectivity within the lattice, not the other way round. Using this concept, a better method of looking for critical regions for $\nu_{crit} < \nu$ is to look for less connected regions, which by definition will have a regional wavelength that is greater than the expected wavelength of the entire lattice. A maximal extremal statistic approach was then taken to find these areas of lower connectivity, by finding the largest possible wavelength for a given ν. Finding these areas of lower connectivity will provide more insight into how AF really forms in lattices of great ν.

Upon inspection of the expression for the analytic $P_{risk,het,\nu}$ (equation 14), it is seen that P_{risk} is inversely proportional to the wavelength ($\lambda_{het,\nu}$). As an overestimate in P_{risk} was observed in the previous method for $\nu_{crit} < \nu$, the wavelength must be an underestimate, further justifying the need to look for the maximal extreme case to address the overestimation of P_{risk} above ν_{crit}.

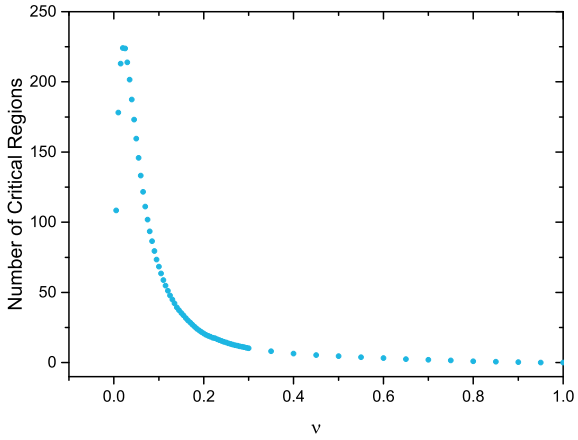

Figure 22: Number of critical regions per ν (N) against ν. The definition of a critical region is defined in equation 2. As $\nu \to 1$, $N \to 0$, and rotors do not form as the connectivity of the lattice becomes the dominant factor in P_{risk}, reducing the relevance of the wavelength.

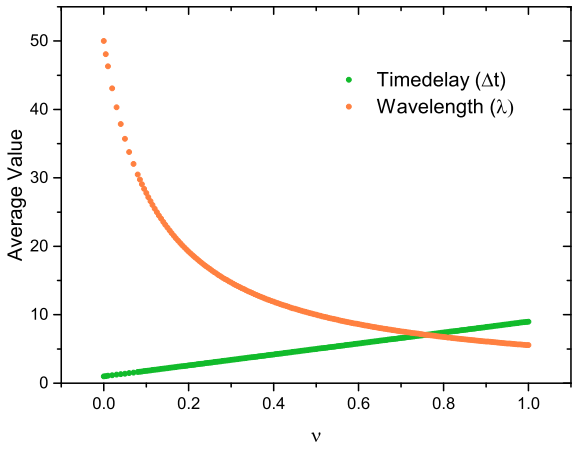

Figure 23: Average timedelay (equation 6) and corresponding wavelength (equation 9) against ν. As $\nu \to 1$, the average wavelength is less able to physically form in that lattice.

The steps to finding P_{risk} using an maximal extremal approach are outlined below for a given lattice of a given ν:

1. Count how many critical defective cells satisfying equation 2 exist in a lattice. This represents the number of critical regions in a lattice (N), which satisfy equation 2 (figure 22)
2. Take a randomly picked cell and record its Δt

3. Repeat step 2 until

$$\sum_{i=1}^{\lambda} \Delta t_i = \tau \tag{15}$$

and record the number of cells required to satisfying equation 15, representative of the wavelength, defined as the minimum number of cells required to form a rotor (λ)

4. Repeat steps 2-3 N times, omitting the cells already picked. This ensures that the sample is representative of how many critical regions there are for a given lattice where N decreases as ν increases (figure 22)
5. Identify the highest value of λ of the lattice (λ_{max})
6. Repeat steps 2-5 for $S = 300$ simulations of the lattice for a given ν
7. Repeat steps 2-8 for all values of ν

For each ν, λ_{max} can be used to obtain a new analytical P_{risk} per ν (figure 24).

$$P_{risk,\nu,max} = 1 - [1 - (1 - \nu)^{2\lambda_{max}}]^{\delta L^2} \tag{16}$$

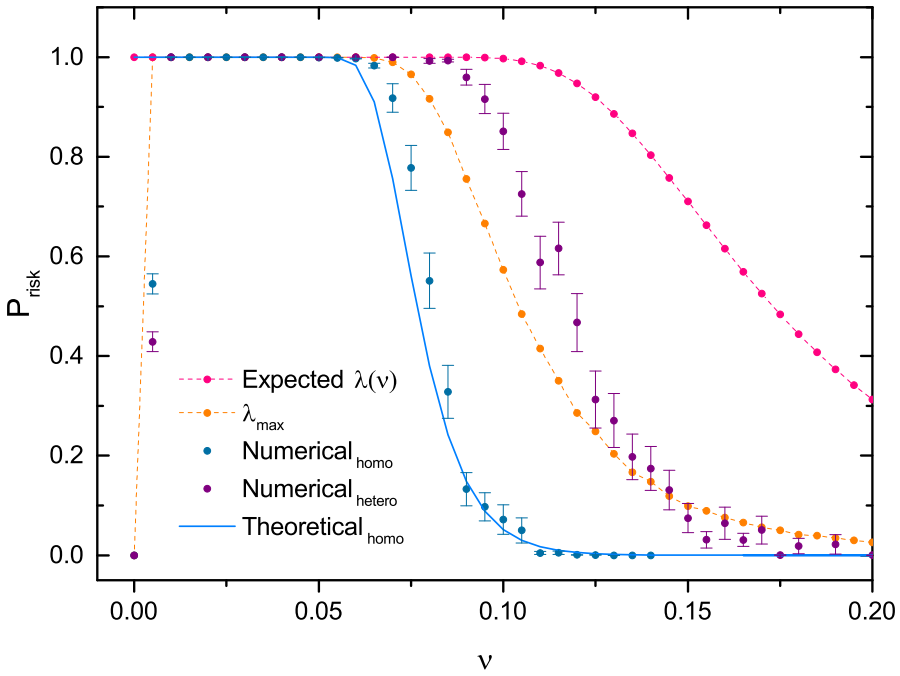

Figure 24: The data obtained from the extremal statistics approach (λ_{max} - orange) is compared against that using the expected wavelength (pink) and the numerical data (purple). The extremal data fits better than the previous fit (pink) for $\nu_{crit} < \nu$ but is now an underestimate around ν_{crit}. There is a clear transition at ν_{crit} where the connectivity for lattice of bigger ν dominates over the wavelength in rotor formation. The extremal fit still deviates too much to be representative of the numerical data in comparison to the analytical fit obtained for Homogeneous CV (blue).

This extremal approach appeared to address the overestimation of P_{risk} for $\nu_{crit} < \nu$ and fits the numerical data better than the expected wavelength fit (figure 24). However for ν around the critical range, the fit is now an underestimate. This is to be expected as maximal statistics were used.

Despite the fit deviating around the critical ν, investigating the extremal case highlighted the concept that as the value of ν increases above ν_{crit}, there is a decrease in the dependence of P_{risk} upon the wavelength. In proceeding with finding the analytical fit for Heterogeneous CV P_{risk}, it is evident that there are structural changes in the lattice as ν exceeds ν_{crit} and the connectivity of the lattice has increased so much that the expected wavelength cannot physically form.

4.2.3 Weighted average of expected wavelength for all ν ($\overline{\lambda}_{het}$)

It was assumed that lattices of all ν had a structure which allows a rotor to form at the expected wavelength (equation 13). As the wavelength is dependent on ν (equation 9), it was naïvely assumed that P_{risk} would reflect the change in wavelength. However, from examining the maximal extreme of the lattice, it was evident that a transition occurs at $\nu_{crit} = 0.1$ above which, underlying structural changes due to increased connectivity mean that the expected wavelength cannot physically form for $\nu_{crit} < \nu$.

Despite the previous argument that rotors are more likely to form for a smaller wavelength (which results from a greater ν), a threshold ν exists, above which the connectivity becomes too dense for rotors at the expected wavelength to form and the expected wavelength becomes more irrelevant in measuring the formation of reentry circuits. Below this threshold, the likelihood of rotor formation remains dependent on the expected wavelength as previously thought. This can explain why the P_{risk} curve drastically decreases above this threshold ν.

Proceeding forward, only the values of ν which yield a non-zero value for the computational P_{risk} ($\nu \leq \nu_{crit}$) have a lattice connectivity which can support reentry circuits. Therefore the numerical value of P_{risk} was used to produced a weighted average wavelength across all ν ($\overline{\lambda}_{het}$), where the weighting acts to suppress wavelength contributions from ν above the threshold discussed above.

1. The weighted average timedelay is given as

$$\overline{\Delta t} = \frac{\sum_{\nu} \langle \Delta t \rangle \cdot P_{het,risk}(\nu)}{\sum_{\nu} P_{het,risk}} \tag{17}$$

2. The weighted average wavelength is then obtained using equation 9

$$\overline{\lambda}_{het} = \frac{\tau}{\Delta t} \tag{18}$$

3. The value of $\overline{\lambda}_{het}$ is then substituted into the analytic expression for Homogeneous P_{risk}, replacing τ (equation 3), to yield analytic values for Heterogeneous P_{risk}

$$P_{risk,het} = 1 - [1 - (1 - \nu)^{2\overline{\lambda}_{het}}]^{\delta L^2} \tag{19}$$

4. As the numerical value of P_{risk} was used for the weighting, steps 1 - 3 are repeated, using the analytic values (step 3) for the weighting instead. Steps 1-3 are iterated until the value of $\overline{\lambda}_{het}$ converges (figure 25)

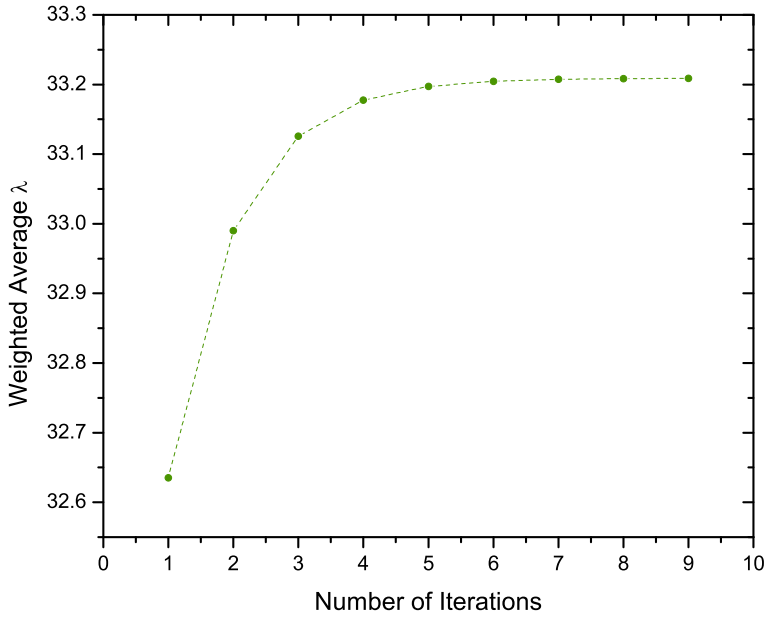

Figure 25: The value of $\overline{\lambda}_{het}$ converges to 33.21 with more iterations of finding the weighted average using the values obtained from equation 19.

The value of $\overline{\lambda}_{het}$ was found to converge to a value of 33.21, verifying that the method was leading somewhere and another analytic expression for Heterogeneous P_{risk} can then be plotted using equation 19 (figure 26) and the newly obtained $\overline{\lambda}_{het}$.

Comparing $\lambda_{hom} = \tau = 50$ to $\overline{\lambda}_{het} = 33.21$, the prediction made in equation 10 is verified in that the minimum path length of a rotor is effectively decreased by implementing Heterogeneous CV. A comparison of the numerical data obtained for all three models discussed in this report as well their corresponding analytic expressions are presented in figure 27.

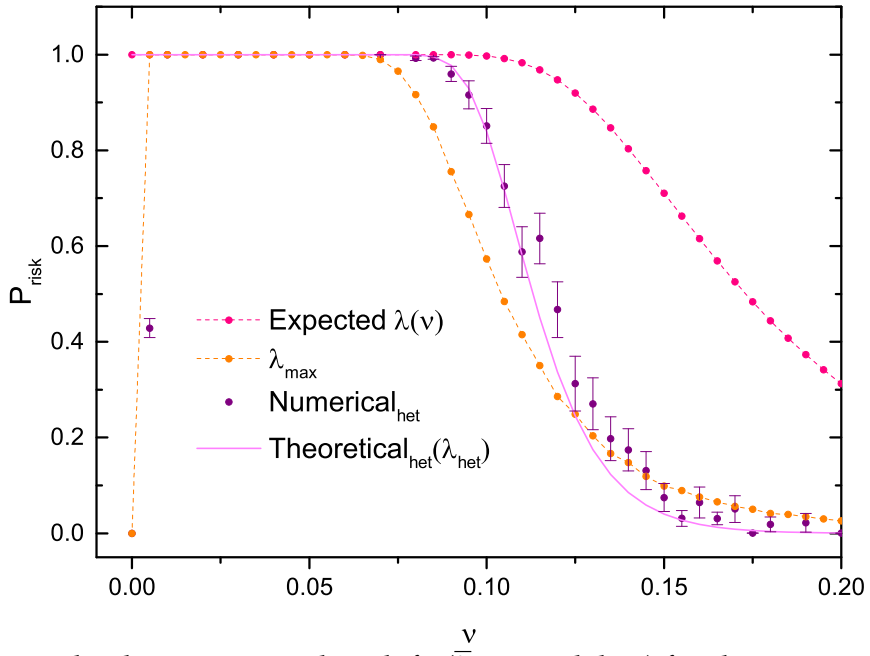

Figure 26: The weighted average wavelength fit ($\overline{\lambda}_{het}$ - pink line) fits the numerical data (purple dots) much better than the previous analytic expressions obtained using expected average wavelength ($\langle\lambda_{het,\nu}\rangle$ - pink dots) and extremal maximum statistics (λ_{max} - orange dots).

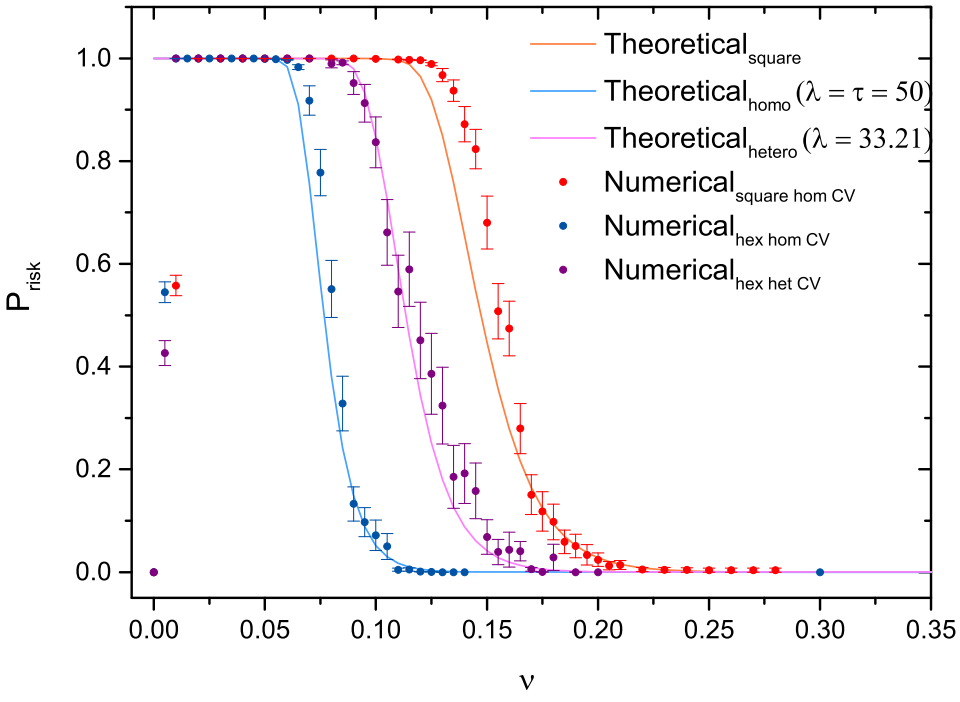

Figure 27: The numerical and analytical values of P_{risk} are shown for $0 \leq \nu \leq 0.3$ for all three models, the Original Square (red), Hexagonal Homogeneous CV (blue) and Hexagonal Heterogeneous CV (purple). The square model has the highest P_{risk} for a given ν but is arguably the most basic representation of the heart.

4.3 Patch Behaviour

4.3.1 Patch of lower ν

As an extension into the investigation of the hexagonal model, the model was returned to Homogeneous CV but still hexagonal, for a basic investigation into fibrosis.

The lattice was set at $\nu = 0,2$, which for a Homogeneous CV hexagonal model has very low, if not zero P_{risk} (figure 16). A patch of a defined radius which had a lower ν (ν_{local}) was then set within the lattice. A series of radii and ν_{local} around the critical ν range, where P_{risk} is non-zero, was investigated (figures 28a and 28b).

Fibrillation was observed to initiate from within the patch which was expected as ν_{local} is at a value known to be at risk of AF. Rotors formed specifically at the patch boundary (figure 28). Dependent on the patch radius as well as ν_{local}, persistent AF then spread out to the whole lattice.

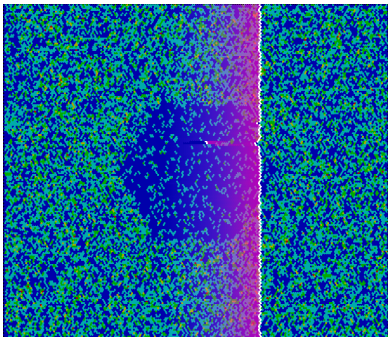

(a) Reentering wavefront from interaction with boundary of patch at $t = 27096$

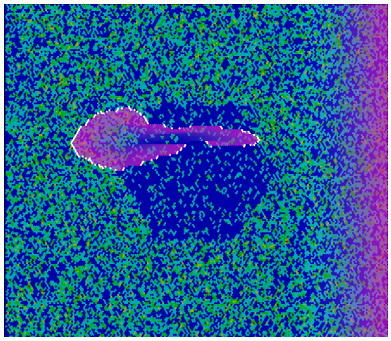

(b) Rotor formation at boundary at $t = 27167$

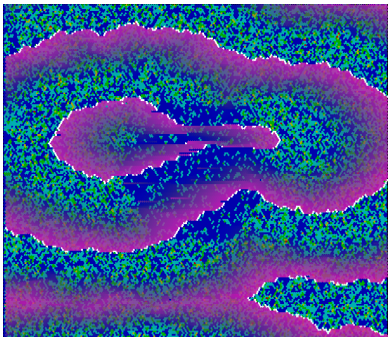

(c) Wavefront of spiral rotors is kinked at boundary of patch at $t = 27818$

Figure 28: Images of model at $\nu = 0.2$ with patch of radius $= 40$ and $\nu_{local} = 0.05$ going into AF. A heat map of connections is shown to represent the underlying structure of the lattice where the connection gradient goes from blue to green to red with increasing connectivity. Using the heat map, the patch of a lower ν_{local} is clearly seen as the bluer region. The interactions of the excited wavefront (white) is seen where the refractory cells (pink) trail behind.The patch boundary appears to induce a reentry circuit which leads to a sustained rotor.

The patch had no effect below a radius of 20 (figure 29a), as reentry circuits which fulfil equation 2 cannot form. A critical radius can therefore be defined equal to $\frac{\tau}{4}$ as the patch diameter is comparable to l_i (equation 2), where it is unlikely, but possible that a reentry circuit forming at one end of the patch can propagate to the very other side.

The patch had a much more suppressed effect when ν_{local} was greater than the $\nu_{crit} = 0.07$ for Homogeneous CV (figure 29b), however a very small chance of AF is possible for patch of radius $= 70$, $\nu_{local} = 0.08$. It is observed that inhomogeneity in connectivity across the lattice does indeed increase the risk of AF forming in what was previously considered a lattice of zero AF risk.

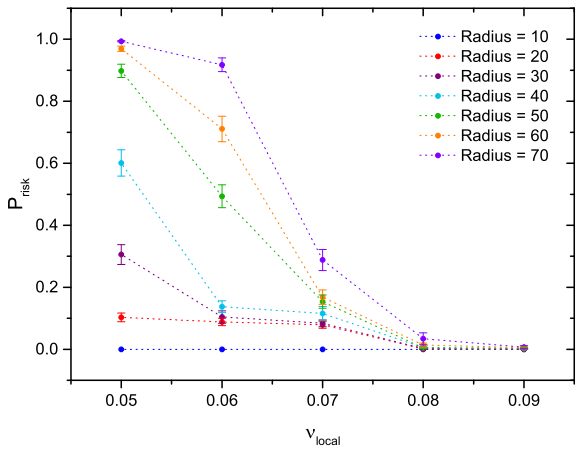

(a) P_{risk} is presented against ν_{local} for several radii.

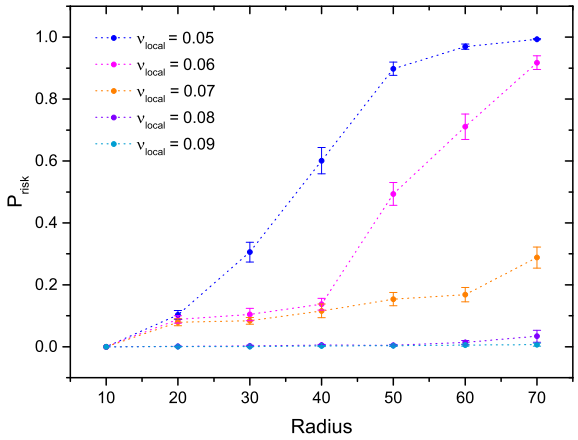

(b) The same data is presented with P_{risk} against patch radius

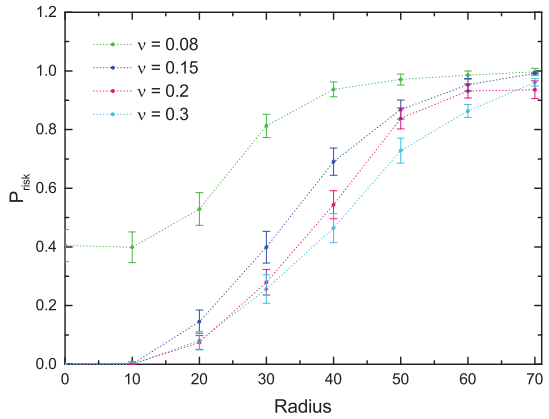

(c) The P_{risk} is presented for a patch at the horizontally-biased percolation threshold

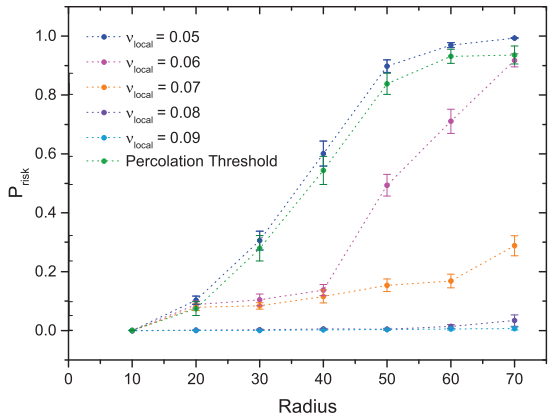

(d) Comparing the percolation patch at $\nu = 0.2$ to the patch at ν_{local}

Figure 29: The data obtained from the Hexagonal Homogeneous CV model with patches of radii of $10, 20, 30, 40, 50, 60$ and 70. **(a)** Patch set at $\nu_{local} = 0.05, 0.06, 0.07, 0.08$ and 0.09, which are known to be at risk of AF for the model whilst the rest of lattice is at non-fibrillatory $\nu = 0.2$. As ν_{local} increases past ν_{crit}=0.07, fibrillation is much harder to induce in the rest of the lattice. The minimum patch size is around 20, as below that, the patch is too small for a reentry circuit to form which fulfils equation 2. **(b)** As the patch gets bigger, the likelihood of inducing AF in the rest of the lattice increases sharply past a critical radius of around 40. This behaviour is not observed for $\nu_{local} > 0.07$ which is the value of ν_{crit} for a hexagonal Homogeneous CV lattice. **(c)** The patch is set at the percolation threshold and the lattice at $\nu = 0.08$ (critical), $0.15, 0.2$ and 0.3. At radius $= 0$, the risk is essentially the same as if no patch were present, and only $\nu = 0.08$ yields a non-zero result as it is around ν_{crit} for the Homogeneous CV model. **(d)** The percolation patch is presented against the patches of ν_{local} and comparable to $\nu_{local} = 0.05$.

4.3.2 Percolating Patch

The P_{risk} was investigated using a patch at horizontally-biased percolation threshold. This time ν for the entire lattice was varied whilst the patch remained at percolation threshold. The P_{risk} was taken for the lattice at $\nu = 0.08, 0.15, 0.2, 0.3$ (figure 29c). For the values of ν known to have zero P_{risk}, the patch set the model into paroxysmal AF for all ν, with a rotor forming at the patch boundary as a result of the excitation wavefront being directed by the percolating patch (figure 30).

Although CV is not implemented for either of the patch investigations, the wavefront was observed to visibly slow down as it moved through the patch. This can be explain by the fact that the connectivity has been reduced down to the percolation threshold, such that the excitation must take a longer path through the patch in order to reach the other side (figure 30). This effect appears to slow the effective conduction velocity, when in actual fact, the cell-to-cell CV remains equal to that outside the patch.

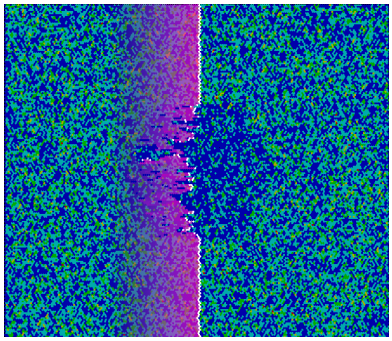

(a) Wavefront propagation through patch at $t = 102$

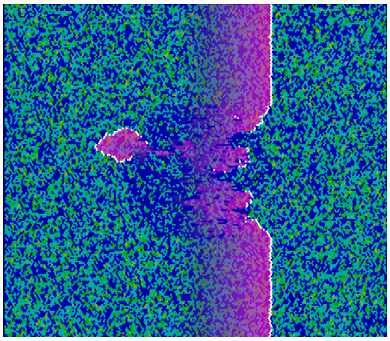

(b) Reentry circuit forms $t = 140$

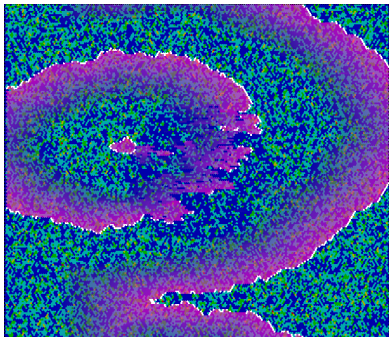

(c) Paroxysmal AF at $t = 297$

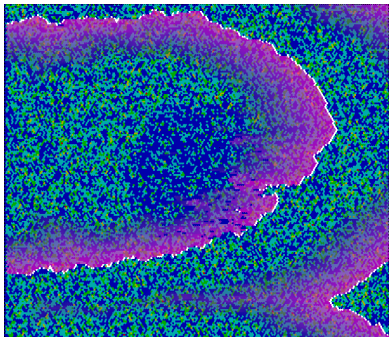

(d) Rotor self-terminates at $t = 500$

Figure 30: At $\nu = 0.2$, with patch at percolation threshold. **(a)** The wavefront takes a longer path through the patch but cell to cell propagation is unchanged. **(b)** Reentry circuit forms as wavefront emerges at patch boundary. **(c)** A single rotor sets the entire lattice into fibrillation. **(d)** The rotor self-terminates indicating paroxysmal fibrillation.

5 Conclusion

The original square model[3] was an accurate representation of the heart, reducing its complex behaviour to its most fundamental level. The model paved the way for this report to continue adding further layers of complexity, one at a time, examining the effects that each layer has upon the way AF induces within the heart.

This report defined two new models in addition to the original, both of which were on a hexagonal lattice, one with homogenous CV (as in the original), and one with heterogeneous CV, where CV is dependent on the cell's coupling. The crossover to the hexagonal model was to better represent the branched nature of real cardiac cells, whilst the introduction of connectivity-dependent CV was to mimic source-sink behaviour[2].

It was found that implementing the model using a hexagonal lattice reduced P_{risk}, this was expected as by introducing a hexagon and the possibility of two new vertical couples, the connectivity of the lattice increased relative to the square model for a given ν. This means a wavefront is more likely to encounter a vertical coupling and is less likely to fulfil equation 2, the condition for reentry, thereby reducing P_{risk}.

Implementing conduction velocity dependent on the cell's connectivity increased the likelihood of AF in comparison to uniform CV. This was because the average propagation speed of the wavefront was reduced and the minimum pathlength required for reentry to occur was effectively reduced too, increasing its likelihood.

Further investigation into the underlying structure revealed that a threshold ν exists, above which the connectivity of the lattice suppresses the formation of rotors as the wavefront cannot reach the required wavelength.

As an extension, this report investigated the effects of implementing a patch of lower connectivity (lower ν), mimicking the effects of atrial fibrosis[4]. The model was returned to homogeneous CV and by varying the size of the patch and the value of ν_{local} it was seen that lattices with a connectivity known to be non-fibrillatory could be induced into fibrillation by rotors which formed at the patch boundary. A critical radius was defined as $\frac{\tau}{4}$ such that the patch was wide enough for reentry circuits to fulfil equation 2 and form self-sustaining rotors. The patch was then set just at the percolating threshold, with horizontal bias such that the wavefront still effectively moved left to right across the lattice and the same effect was observed.

5.1 Future Discussion

The representation of source-sink behaviour[2] was implemented in its most basic level as the propagation of charge was discretised and only the connecitivity of the excited cell was considered. Given more time, to make the model more realistic, the connectivity of the excited cell and that of its connected neighbours could be considered. This would represent pouring water into many leaking bucket with holes rather than just many buckets

and would act to make the flow of charge more continuous.

Another area that deserves more investigation would be the patches of lower ν. Given more time, the patches could be investigated using the heterogeneous CV model. As risk is greater and wavelength is smaller, it would be insightful to see if the smallest patches could induce AF throughout the lattice, analogous to the early stages of fibrosis.

This report aimed to investigate different aspects of inhomogeneity. Whether it be the cell connectivity as a result of fibrosis or the conduction velocity, clearly the recurring theme of inhomogeneity is crucial in the initiation and sustenance of AF in the myocardium. The results obtained were related to the physical and biological representations and have furthered the insight into the critical structures that are underlying in AF mechanisms which can hopefully pave the way for new treatment with a greater success rate.

6 Acknowledgements

First and foremost I would like to thank Professor Kim Christensen for his invaluable insight provided the guidance to oversee us throughout our journey over this past year.

Secondly, much gratitude and admiration goes towards Kishan Manani whose contribution towards the original model provided the inspiration for us to follow. His guidance made this project easier to tackle.

Finally I would like to thank my project partner not only for their fabulous programming skills and sharp analytical mind, which made our model so efficient, but also for being a pillar of support and an oasis of calm during this tumultuous year.

References

[1] U Schotten, S Verheule, P Kirchhof, and A Goette. Pathophysiological mechanisms of atrial fibrillation: a translational appraisal. *Physiological reviews*, 91(1):265–325, January 2011.

[2] P Spector. Principles of cardiac electric propagation and their implications for re-entrant arrhythmias. *Circulation. Arrhythmia and electrophysiology*, 6(3):655–61, June 2013.

[3] K Christensen, K A Manani, and N S Peters. Simple Model for Identifying Critical Regions in Atrial Fibrillation. *Physical Review Letters*, 114(2):028104, January 2015.

[4] B Burstein and S Nattel. Atrial fibrosis: mechanisms and clinical relevance in atrial fibrillation. *Journal of the American College of Cardiology*, 51(8):802–9, February 2008.

[5] Texas Heart Institute Health Information Center, `http://www.texasheart.org/HIC/Topics/Cond/Arrhythmia.cfm`. Accessed: 1 September 2014.

[6] S Nattel. New ideas about atrial fibrillation 50 years on. *Nature*, 415(6868):219–26, January 2002.

[7] E Braunwald. Structure and function of the normal myocardium. *British heart journal*, 33:Suppl:3–8, January 1971.

[8] J Pinnell, S Turner, and S Howell. Cardiac muscle physiology. *Continuing Education in Anaesthesia, Critical Care & Pain*, 7(3):85–88, May 2007.

[9] H Winterberg. Studien über Herzflimmern. *Pflüger, Archiv für die Gesammte Physiologie des Menschen und der Thiere*, 117(3-4):223–256, March 1907.

[10] G R Mines. On circulating excitations in heart muscles and their possible relation to tachycardia and fibrillation. *Trans R Soc Can*, 8:43–52, 1914.

[11] W E Garrey. Auricular Fibrillation. *Physiol Rev*, 4(2):215–250, April 1924.

[12] G R Mines. On dynamic equilibrium in the heart. *The Journal of physiology*, 46(4-5):349–83, July 1913.

[13] D Scherf, F J Romano, and R Terranova. Experimental studies on auricular flutter and auricular fibrillation. *American Heart Journal*, 36(2):241–251, August 1948.

[14] G K Moe and J A Abildskov. Atrial fibrillation as a self-sustaining arrhythmia independent of focal discharge. *American heart journal*, 58:59–70, 1959.

[15] M A Allessie, F I Bonke, and F J Schopman. Circus movement in rabbit atrial muscle as a mechanism of tachycardia. III. The "leading circle" concept: a new model of circus movement in cardiac tissue without the involvement of an anatomical obstacle. *Circulation research*, 41(1):9–18, July 1977.

[16] J Beaumont, N Davidenko, J M Davidenko, and J Jalife. Spiral waves in two-dimensional models of ventricular muscle: formation of a stationary core. *Biophysical journal*, 75(1):1–14, July 1998.

[17] A C Skanes, R Mandapati, O Berenfeld, J M Davidenko, and J Jalife. Spatiotemporal periodicity during atrial fibrillation in the isolated sheep heart. *Circulation*, 98(12):1236–48, September 1998.

[18] J Jalife. Rotors and spiral waves in atrial fibrillation. *Journal of cardiovascular electrophysiology*, 14(7):776–80, July 2003.

[19] C A Morillo, G J Klein, D L Jones, and C M Guiraudon. Chronic rapid atrial pacing. Structural, functional, and electrophysiological characteristics of a new model of sustained atrial fibrillation. *Circulation*, 91(5):1588–95, March 1995.

[20] M Haïssaguerre, P Jaïs, D C Shah, A Takahashi, M Hocini, G Quiniou, S Garrigue, A Le Mouroux, P Le Métayer, and J Clémenty. Spontaneous initiation of atrial fibrillation by ectopic beats originating in the pulmonary veins. *The New England journal of medicine*, 339(10):659–66, September 1998.

[21] J L Cox, J P Boineau, R B Schuessler, R D Jaquiss, and D G Lappas. Modification of the maze procedure for atrial flutter and atrial fibrillation. I. Rationale and surgical results. *The Journal of thoracic and cardiovascular surgery*, 110(2):473–84, August 1995.

[22] S J Melby, A Zierer, M S Bailey, J L Cox, J S Lawton, N Munfakh, T D Crabtree, Nader Moazami, Charles B Huddleston, Marc R Moon, and Ralph J Damiano. A new era in the surgical treatment of atrial fibrillation: the impact of ablation technology and lesion set on procedural efficacy. *Annals of surgery*, 244(4):583–92, October 2006.

[23] J Kneller and S Nattel. How do class I antiarrhythmic drugs terminate atrial fibrillation? A quantitative analysis based on a realistic ionic model (abstract). *Circulation*, 104:II–5, 2001.

[24] S Nattel. Experimental evidence for proarrhythmic mechanisms of antiarrhythmic drugs. *Cardiovascular research*, 37(3):567–77, March 1998.

[25] A L Hodgkin and A F Huxley. A quantitative description of membrane current and its application to conduction and excitation in nerve. *The Journal of physiology*, 117(4):500–44, August 1952.

[26] R H Clayton. Computational models of normal and abnormal action potential propagation in cardiac tissue: linking experimental and clinical cardiology. *Physiological measurement*, 22(3):R15–34, August 2001.

[27] G K Moe, W C Rheinboldt, and J A Abildskov. A COMPUTER MODEL OF ATRIAL FIBRILLATION. *American heart journal*, 67:200–220, 1964.

[28] M Gerhardt, H Schuster, and J Tyson. A cellular automation model of excitable media including curvature and dispersion. *Science*, 247(4950):1563–1566, March 1990.

[29] G Bub, L Glass, N G Publicover, and A Shrier. Bursting calcium rotors in cultured cardiac myocyte monolayers. *Proceedings of the National Academy of Sciences*, 95(17):10283–10287, August 1998.

[30] G Bub, A Shrier, and L Glass. Spiral wave generation in heterogeneous excitable media. *Physical review letters*, 88(5):058101, February 2002.

[31] Z Qu, F Xie, A Garfinkel, and J N Weiss. Origins of Spiral Wave Meander and Breakup in a Two-Dimensional Cardiac Tissue Model. *Annals of Biomedical Engineering*, 28(7):755–771, July 2000.

[32] S Alonso and M Bär. Reentry Near the Percolation Threshold in a Heterogeneous Discrete Model for Cardiac Tissue. *Physical Review Letters*, 110(15):158101, April 2013.

[33] Tokai University, `http://edu.icc.u-tokai.ac.jp/cos/3year/system/histology/histology/atlas/Circulatory-system/myocardium1.jpg`. Accessed: 1 April 2015.

[34] Cardiac Tissue Diagram, `http://anatomybodypart.com/human-muscle-tissue-diagram/muscle-tissue-types-3/`. Accessed: 1 April 2015.

Appendices

A Derivation of analytical P_{risk} expression

P_{risk} is the probability that at least one defective cell in a lattice is critical. The analytical expression for a hexagonal model is given by equation 3 and the derivation is explained here, having been adapted from the square lattice by Christensen *et al*[3].

For a defective cell to be critical, the distance from a defective cell to the next vertically coupled cell (l_i) must satisfy

$$(l_i) > \frac{\tau}{2} \tag{20}$$

The probability of a given cell having one vertical couple is ν.

The probability of a given cell *not* having one vertical couple is $1 - \nu$.

There are 4 possible vertical couples on a hexagon and so the probability that a given cell has *no vertical couples at all* is

$$(1 - \nu)^4 \tag{21}$$

The probability that a given cell has *at least one* vertical couple is

$$1 - (1 - \nu)^4 \tag{22}$$

The probability that a defective cell satisfies equation 20 is

$$\sum_{i=0}^{\frac{\tau}{2}-1} (1 - p_\nu)^{l_i} p_\nu = 1 - (1 - \nu)^{2\tau} \tag{23}$$

There are δL defective cells in an $L \times L$ lattice

The probability that *all* the defective cells satisfiy equation 20 is

$$[1 - (1 - \nu)^{2\tau}]^{\delta L^2} \tag{24}$$

The probability that *at least one* defective cell in a **hexagonal** lattice satisfies equation 20 is

$$P_{risk,hex} = 1 - [1 - (1 - \nu)^{2\tau}]^{\delta L^2} \tag{25}$$

A.1 Original Square Model

For a square lattice, there are only 2 possible vertical couplings and so equation 21 is rewritten as

$$(1-\nu)^2 \tag{26}$$

Following through the rest of the derivation yields the probability that *at least one* defective cell in a **square** lattice satisfies equation 20 is

$$P_{risk,sq} = 1 - [1-(1-\nu)^{\tau}]^{\delta L^2} \tag{27}$$

B Error Handling

The average over N simulations is given by $\overline{x}$

$$\overline{x} = \frac{1}{N}\sum_{i=1}^{N} x_i \tag{28}$$

and the associated error for the $\overline{x}$ is given by the standard error of the mean

$$SE_{\overline{x}} = \frac{\sigma}{\sqrt{N}} \tag{29}$$

using the unbiased sample Standard Deviation (σ).

$$\overline{\sigma} = \frac{1}{N-1}\sum_{i=1}^{N}(x_i - \overline{x})^2 \tag{30}$$

C Code

All the code used in simulating the project can be found online at `https://github.com/bethhallowell/MSci-Project` as there were too many lines to physically include in this project. The original square model can be found under OriginalSquareModel.cpp, the final code which includes the hexagonal and conduction velocity features can be found under FinalMergedCAModel.cpp. The code for the detection of critical regions and the extremal statistics test can be found under ExtremalStatistics.cpp. Additionally, a header file HelperFunctions.h is included which is required for the code to run as well the cpp and header files for the Mersenne Twister random number generator. The visualisation was performed using SFML library which can be downloaded from here `http://www.sfml-dev.org/download.php`, and is required for the code to compile correctly.